Title

Distinct Source Water Chemistry Shapes Contrasting Concentration-Discharge Patterns

Journal

Water Resources Research, 55(5)

ISSN

0043-1397

Authors

Zhi, Wei

Li, Li

Dong, Wenming

et al.

Publication Date

2019-05-01

DOI

10.1029/2018wr024257

Peer reviewed

Distinct Source Water Chemistry Shapes Contrasting Concentration-Discharge Patterns

Wei Zhi[1], Li Li[2], Wenming Dong[3], Wendy Brown[4], Jason Kaye[5], Carl Steefel[3], and Kenneth H. Williams[3,4]

[1] Department of Energy and Mineral Engineering, The Pennsylvania State University, University Park, PA, USA, [2] Department of Civil and Environmental Engineering, The Pennsylvania State University, University Park, PA, USA, [3] Earth and Environmental Sciences Area, Lawrence Berkeley National Laboratory, Berkeley, CA, USA, [4] The Rocky Mountain Biological Laboratory, Crested Butte, CO, USA, [5] Department of Ecosystem Science and Management, The Pennsylvania State University, University Park, PA, USA

Correspondence to: L. Li, lili@engr.psu.edu

Abstract

Understanding concentration-discharge (C-Q) relationships are essential for predicting chemical weathering and biogeochemical cycling under changing climate and anthropogenic conditions. Contrasting C-Q relationships have been observed widely, yet a mechanistic framework that can interpret diverse patterns remains elusive. This work hypothesizes that seemingly disparate C-Q patterns are driven by switching dominance of end-member source waters and their chemical contrasts arising from subsurface biogeochemical heterogeneity. We use data from Coal Creek, a high-elevation mountainous catchment in Colorado, and a recently developed watershed reactive transport model (BioRT-Flux-PIHM). Sensitivity analysis and Monte-Carlo simulations (500 cases) show that reaction kinetics and thermodynamics and distribution of source materials across depths govern the chemistry gradients of shallow soil water and deeper groundwater entering the stream. The alternating dominance of organic-poor yet geo-solute-rich groundwater under dry conditions and organic-rich yet geo-solute-poor soil water during spring melt leads to the flushing pattern of dissolved organic carbon and the dilution pattern of geogenic solutes (e.g., Na, Ca, and Mg). In addition, the extent of concentration contrasts regulates the power law slopes (*b*) of C-Q patterns via a general equation $b = \frac{\delta_b \, C_{ratio}}{C_{ratio,1/2}+C_{ratio}} + b_{min}$. At low ratios of soil water versus groundwater concentrations ($C_{ratio} = C_{sw}/C_{gw} < 0.6$), dilution occurs; at high ratios ($C_{ratio} > 1.8$), flushing arises; chemostasis occurs in between. This equation quantitatively interprets *b* values of 11 solutes (dissolved organic carbon, dissolved P, NO_3^-, K, Si, Ca, Mg, Na, Al, Mn, and Fe) from three catchments (Coal Creek, Shale Hills, and Plynlimon) of differing climate, geologic, and land cover conditions. This indicates potentially broad regulation of subsurface biogeochemical heterogeneity in determining C-Q patterns and wide applications of this equation in quantifying *b* values, which can have broad implications for predicting chemical weathering and biogeochemical transformation at the watershed scale.

1 Introduction

Watersheds act as reactors that incubate interactions among soil, roots, microbes, and water, ultimately connecting the land to aquatic systems on Earth (Grathwohl et al., 2013). Solute concentrations (C) and discharge (Q) at stream outlets integrate hydrological and reaction processes and bear convoluted signature at the watershed scale. C-Q relationships have been extensively used to understand watershed structure and function (Musolff et al., 2015), to quantify chemical weathering (White & Blum, 1995), and to illuminate watershed response to changing climate and human perturbations (Stackpoole et al., 2017). Similar C-Q patterns have been observed for different solutes across watersheds; varying C-Q patterns have been observed for different solutes in the same watershed and for the same solute in different watersheds (Godsey et al., 2009; Herndon et al., 2018; Musolff et al., 2017; Winnick et al., 2017). Several schools of thought exist to explain disparate C-Q behaviors, emphasizing the importance of flow paths (Hornberger et al., 1994), connectivity (Pacific et al., 2010), residence time (Maher, 2011), reaction kinetics (Ameli et al., 2017; Li, Bao, et al., 2017), ion exchange (Clow & Mast, 2010), vegetation (Herndon et al., 2015a), and temperature (Winterdahl et al., 2014). To date, these diverse and site-specific explanations have not been integrated into an overarching framework that would facilitate the development of a coherent theory with predictive power.

Studies of C-Q date back to more than five decades for understanding event-based C-Q hysteresis (Evans & Davies, 1998; Johnson et al., 1969). The simple power law $C = aQ^b$ has been extensively used to classify C-Q patterns (Godsey et al., 2009), although recent work has proposed more detailed characterization (Moatar et al., 2017; Zhang, 2018). Chemostasis is defined as relatively small variations in concentrations compared to discharge, with values of b between -0.1 and 0.1 and/or relatively small coefficients of variance (CV < 1) compared to discharge (CV_c/CV_Q; Musolff et al., 2015; Thompson et al., 2011). Chemodynamic patterns are characterized as having high absolute b values (>0.1) and large CV_c/CV_Q values (>1). Positive b values indicate increasing concentrations with discharge, that is, flushing or enrichment behavior, whereas negative b values allude to decreasing concentrations with discharge or dilution behavior.

Geogenic species (e.g., Na, Mg, and Si) derived from chemical weathering have demonstrated widespread chemostatic behavior (Godsey et al., 2009). Yet exceptions do exist, manifesting significant dilution of Ca and Na in regions with high runoff (Moon et al., 2014) and flushing patterns of Ca, Mg, and Na at a site where cation-rich water from silicate weathering in shallow layers contributed most to the stream at high flows (Bhat et al., 2016). For dissolved organic carbon (DOC), flushing behaviors are commonly observed (Boyer et al., 1997; Musolff et al., 2017), although slight dilution is notable where net primary productivity or carbon source are limited (Zarnetske et al., 2018). Nitrogen has demonstrated as flushing patterns in forests (Creed

et al., 1996; Creed & Band, 1998). In agricultural land, however, chemostatic patterns are the norm (Basu et al., 2010; Thompson et al., 2011) except where groundwater dominates its export (Miller et al., 2016; Musolff et al., 2016). Total phosphorous (TP) commonly displays flushing patterns owning to high particulate P level in shallow soils at high discharge (Haygarth et al., 2004).

The C-Q literature has been teeming with rich and diverse explanations for disparate C-Q patterns. Chemostasis has been attributed to hydrologically responsive dissolution rates (via wet surface area; Li, Bao, et al., 2017), buffering capacity of ion exchange reactions (Clow & Mast, 2010), and approaching to equilibrium as residence time increases (Ameli et al., 2017; Maher, 2011). Flushing behaviors have been attributed to rising water tables tapping shallow soils with enriched organic carbon and nutrients, increased hydrological connectivity between uplands and streams under high flow conditions, and control of source element distribution and varying temperature (Herndon et al., 2015a; Pacific et al., 2010; Seibert et al., 2009; Winterdahl et al., 2014). Dilution behaviors have been attributed to high groundwater concentration that is diluted by rainwater at high discharge (Li, Bao, et al., 2017; Miller et al., 2016), short residence time for dissolution, and rapid depletion of solute stores (Herndon et al., 2015b; Hoagland et al., 2017). Musolff et al. (2017) attribute distinct C-Q patterns to spatial structure heterogeneity of source waters and travel times for different extent of transformation reactions in a watershed.

Despite diverse explanations, a growing consensus on the hydrological controls of C-Q relationships has emerged. In particular, stream water mixes different types of water, primarily shallow soil water (e.g., perched water table) and relatively deep groundwater and occasionally precipitation water. The dominance of shallow versus deep water varies under wet and dry conditions. Disproportionally high DOC and nutrient exports during storms suggest shallow soil water as a major source and key driver of variable stream concentration (Boyer et al., 1997; Pacific et al., 2010; Seibert et al., 2009). On the other hand, at dry times, the dominance of groundwater brings with it high level of geogenic species from depths (Kim et al., 2014). The chemistries of deep and shallow groundwater typically differ, with the extent of difference defined particularly by the subsurface biogeochemical property contrasts along depth (Herndon et al., 2018; Sullivan et al., 2016). Similarly, horizontal spatial heterogeneity (e.g., wetland vs. hillslope; swale vs. planar slopes) or the proximity of source zones to streams often controls their connectivity to streams under different flow regimes and regulates stream chemistry (Herndon et al., 2015b; Schwab et al., 2017).

This consensus has emerged piecemeal from a variety of measurements and observations, but it has not been woven together as an overarching framework to unify diverse explanations. Part of the reason is that with complex hydro-biogeochemical processes masked by spatial heterogeneities, field measurements are often only partially useful because water and water

chemistry data often reflect a convoluted signature that cannot distinguish causes and effects (Weiler & McDonnell, 2006). In addition, there has been a lack of modeling tools that integrate hydrological and biogeochemical processes. Historically, hydrologists and biogeochemists have been developing models along two separate lines: hydrology models focusing on catchment hydrological processes and reactive transport models focusing on coupled transport and reactions with rigorous kinetics and thermodynamics (Fatichi et al., 2016; Li, Maher, et al., 2017). Our recently developed RT-Flux-PIHM couples a reactive transport model with a watershed hydrology model, offering a tool for process integration across disciplines (Bao et al., 2017; Li, Bao, et al., 2017; Li, Maher, et al., 2017). RT-Flux-PIHM includes abiotic geochemical reactions (e.g., mineral dissolution and precipitation, ion exchange, and aqueous and surface complexations) to understand the dynamics of geogenic species (i.e., Ca and Mg) driven by chemical weathering. This code has been augmented in this work to BioRT-Flux-PIHM with the addition of microbe-mediated biogeochemical redox reactions (e.g., decomposition of organic matters, denitrification, and iron and sulfate reductions) to simulate processes relevant to biogenic solutes, such as DOC and nitrogen. This can test disparate mechanisms of diverse C-Q behaviors. Here we hypothesize that seemingly disparate C-Q behaviors are driven by the relative dominance of different source waters under different hydrological regimes with distinct chemistry arising from subsurface biogeochemical heterogeneity. Such complex interactions may never be tractably tested with field studies. Here we apply BioRT-Flux-PIHM to Coal Creek, a high-elevation catchment in central Rocky Mountain of Colorado that is vulnerable to warming and shrinking snow fractions. We further cast the findings from Coal Creek to broader conditions combining sensitivity analysis, Monte-Carlo simulations, and comparison with data from other watersheds.

2 The Study Site

This field site Coal Creek is a headwater high-elevation catchment in the central Rocky Mountains of Colorado, USA. It is a third-order stream in Gunnison County and drains an area of approximately 53 km^2 about 200-km southwest of Denver (Figure 1a). It originates from the Ruby mining district near Lake Irwin and flows east toward the town of Crested Butte before entering the Slate River, a tributary of the East River that ultimately joins the Gunnison River (Hubbard et al., 2018). This mountainous watershed is part of the Ruby-Anthracite Range with elevations from 2,700 m in Crested Butte to about 3,700 m for the northwestern peaks of the Ruby Range (Figure 1a). Average slope calculated by ArcMap (v10.3) is 16°. The mean annual temperature is around 0.9 °C. Data from the local weather station at Crested Butte (latitude: 38.8738, longitude: −106.977; http://www.usclimatedata.com/) indicate annual average rainfall and snowfall of 612 mm and 551 cm, respectively. The watershed is seasonally snow-covered from approximately mid-November to mid-June with a maximum

ground snowpack of >150 cm typically in mid-February, after which the snowmelt dominates. Coal Creek is therefore a representative high-elevation mountain watershed that supplies the majority of surface water in the Western United States, similar to the neighboring East River watershed (Hubbard et al., 2018). It is vulnerable to diminishing snow fraction in winter and decreasing snowmelts in the summer (Berghuijs et al., 2014; Carroll et al., 2018). The watershed consists primarily of evergreen forest (65%) and herbaceous vegetation (20%), followed by deciduous forest (9%), barren land (3%), and woody wetland (3%; Figure 1b).

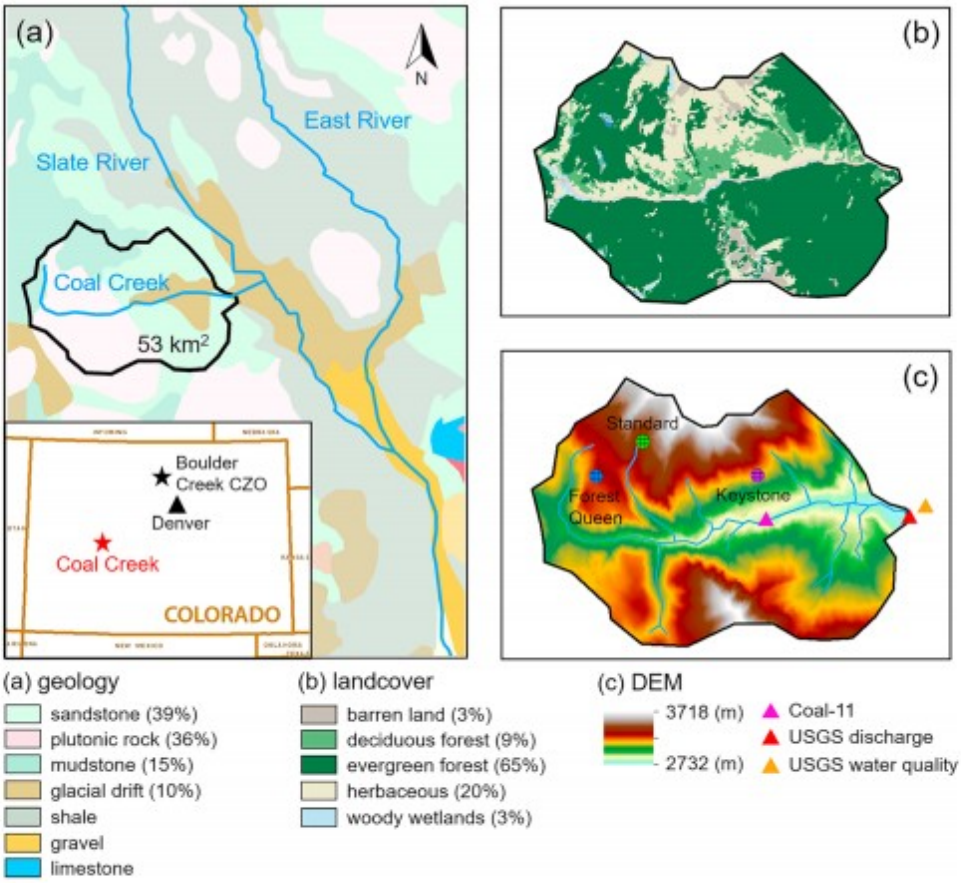

Figure 1. Coal Creek watershed: (a) location and geology; (b) land cover; and (c) Digital Elevation Map (DEM) and sampling locations. Coal Creek is a high-elevation watershed, about 200-km southwest of Denver, and is a tributary of Slate River. USGS = United States Geological Survey.

The lithology includes primarily sandstone (39%) and mudstone (15%; Figure 1a) that belong to the Mesaverde, Tertiary Wasatch, and Ohio Creek Formations (Manning et al., 2008; Streufert, 1999). Plutonic rock (36%) originated during the Middle Tertiary, when the Red Lady stock was emplaced under Mt Emmons and widespread volcanism occurred south of the study area. A small area (10%) in the valley is covered by Quaternary Glacial Drift, which consists of various surficial deposits including unsorted glacial till and associated sand and gravel deposits. The Ruby mining district

was mined for metals between 1874 and 1974 primarily in the Standard Mine, Keystone Mine, and Forest Queen Mine (Figure 1c; Shanklin & Ryan, 2006). Although mining activities have ceased, heavy metals continue to flush into Coal Creek, which supplies drinking water to Crested Butte. The likely sources of Zn, Mn, and Cd are inferred to be shale interbeds rich in organic materials and primary and secondary pyrite and metal sulfides (Streufert, 1999; Thomas & Galey, 1982). Sphalerite ((Zn,Fe)S) and manganese oxides have been identified (Manning et al., 2008). Sphalerite regularly contains small percentages of Cd as it can substitute for Zn. Manganese enrichment is common in porphyry-type molybdenum deposits, such as those that underlie the nearby Mt. Emmons molybdenum porphyry deposit. Concentrations of trace metals in Coal Creek are one to two orders of magnitude higher than those in groundwater, possibly caused by residual mine tailings and small iron fen tributaries draining into the river directly.

3 Methods

In this work, we collected new data and also used existing water and solute data from the United States Geological Survey (USGS). We simulate hydrological processes to understand the water cycle and biogeochemical processes of DOC and Na as two representative solutes with flushing and dilution behaviors. Sensitivity analyses were carried out to understand the role of reaction kinetics and thermodynamics in determining C-Q relationships. Monte-Carlo simulations of 500 runs that randomly sampled across the uncertainty range of soil and groundwater concentrations were conducted to extrapolate to broader conditions.

3.1 Water and Water Chemistry Data

The USGS has monitored daily streamflow of Coal Creek at Crested Butte since October 2014 (site ID: 09111250). USGS water data (site ID: 385224106590100) were retrieved from the Water Data website (https://waterdata.usgs.gov/usa/nwis/), including DOC, total unfiltered nitrogen (TN), total unfiltered organic nitrogen (TON), geogenic solutes (e.g., Na, Mg, and Ca), chloride (Cl), and trace metals (e.g., Zn, Mn, and Cd). The discharge station is operated from 1 April to 15 November. Snow data including snowpack thickness and snow water equivalent (SWE) were retrieved from the U.S. Department of Agriculture (USDA) Snow Telemetry (SNOTEL) database (https://www.wcc.nrcs.usda.gov/snow/) at Crested Butte (#380). Groundwater chemistry at a depth of 9 meters is measured at Crested Butte from December 1996 to May 2012 (U. S. Geological Survey (USGS) site ID: 385213106584700).

Stream chemistry data include two sets of measurements: the long-term low-frequency (once every 2 months) measurements (LFM) by the USGS from November 2000 to December 2016 and our own high-frequency measurements (HFM) sampled at Coal-11 (Figure 1c) every other day from April to October and every week from November to March since 2016. The LFM record reveals the trend in the past decade, while the HFM data

illuminate the dynamics of individual snowmelt seasons in the past couple of years. A total of >40 solutes is measured, as listed in supporting information Text S1. Detailed sampling and measurements are also discussed in Supporting Information S1. For this work, we primarily focus on carbon, nutrients, and a few representative geogenic and trace metal solutes.

3.2 BioRT-Flux-PIHM: A Watershed Biogeochemical Reactive Transport Model

Here we present essential features of BioRT-Flux-PIHM, one of the models in the PIHM family code (Duffy et al., 2014), that help understand the rest of the paper. It includes microbe-mediated redox reactions based on RT-Flux-PIHM (Figure 2; Bao et al., 2017). The model couples three modules: a multicomponent reactive transport module BioRT, the land-surface interaction module Flux for processes such as solar radiation and evapotranspiration (ET), and the surface hydrology module PIHM for hydrological processes (e.g., precipitation, infiltration, recharge, surface runoff, and subsurface flow). The BioRT module takes in the computed water fluxes and storage from Flux-PIHM and simulates processes including advection, diffusion, dispersion, and biogeochemical reactions and outputs aqueous and solid concentrations. The reactions can be kinetics-controlled (mineral dissolution and precipitation and microbe-mediated reactions) and thermodynamically controlled (e.g., ion exchange, surface complexation [sorption], and aqueous complexation). Flux-PIHM solves for water-related variables including water storage, flow, soil moisture, and water table depth. For subsurface flow, the model distinguishes between active interflow in shallow soil zones and groundwater flow that is relatively shallow and is connected to the stream but is deeper than soil (Figure 2).

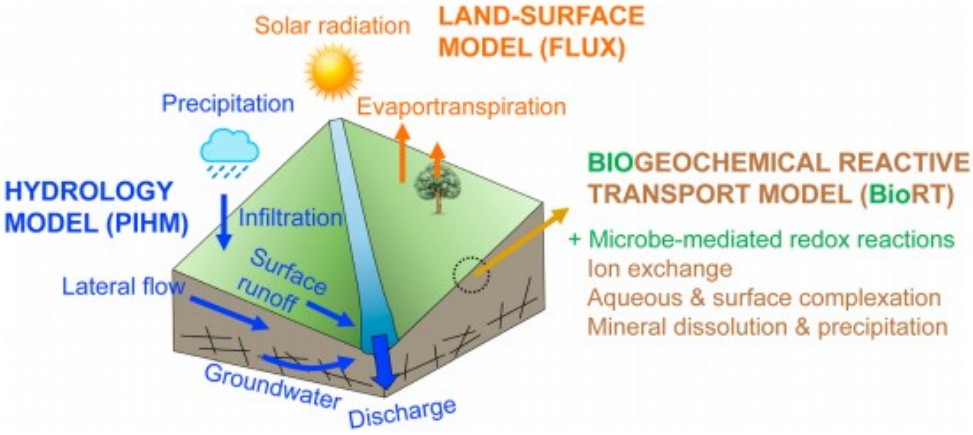

Figure 2. A schematic representation of processes in different modules (different colors) in BioRT-Flux-PIHM. Discharge comes from surface runoff, subsurface lateral flow, and shallow groundwater. The model is augmented based on the RT-Flux-PIHM (Bao et al., 2017). The new addition of the model in this work is the microbe-mediated biogeochemical redox reactions in BioRT. These reactions include but are not limited to organic carbon decomposition, mineralization, nitrification, and denitrification.

The governing equation for an arbitrary solute *m* in grid *i* is as follows (Bao et al., 2017):

$$V_i \frac{\mathrm{d}\left(S_{w,i}\theta_i C_{m,i}\right)}{\mathrm{d}t} = \sum_{j=N_{i,1}}^{N_{i,x}} \left(A_{ij} D_{ij} \frac{C_{m,j} - C_{m,i}}{I_{ij}} - q_{ij} C_{m,j} \right) + R_{m,i}, \qquad m = 1, \ldots, np \quad (1)$$

where V_i is the total volume of the grid i (solid + liquid volume; m^3); $S_{w,i}$ is soil water saturation (m^3 water per m^3 pore space); θ_i is porosity (m^3 pore space per m^3 total volume); $C_{m,i}$ is the aqueous concentration of species m (mol/m^3 water); $N_{i,x}$ is the index of neighboring elements of i sharing interface; the value of x is two for the unsaturated zone (infiltration and recharge) and four for the saturated zone (recharge plus three lateral flow directions), respectively; A_{ij} is the interface area (m^2) shared by i and its neighbor grid j; D_{ij} is the combined dispersion/diffusion coefficient (m^2/s) normal to the shared surface A_{ij}; I_{ij} is the distance between the center of i and its neighbor elements j; q_{ij} is the flow rate across A_{ij} (m^3/s); R_m is the summation of rates of kinetically controlled reactions that involve species m (mol/s) of a total of np primary solute species.

Microbe-mediated reactions include, for example, decomposition of soil organic carbon (SOC) and nutrients, nitrification, and denitrification. The BioRT module is written such that users can define specific reactions to be simulated via input files and the geochemical database. BioRT implements the general dual-substrate Monod kinetics with inhibition terms that can simulate the biogeochemical redox ladder (Li et al., 2009; Monod, 1949). The dual-Monod and inhibition term may become important under conditions where carbon and/or electron acceptors are limited, especially in groundwater systems. In this work, however, because carbon decomposition occurs in soils often with ample SOC as the electron donor and O_2 as the electron acceptor, these terms are typically not important and are therefore ignored. The rate law of microbe-mediated redox reactions in this work therefore is simplified to the following:

$$r_{\mathrm{bio}} = kAf(Z_w)f(T)f(S_w), \quad (2)$$

where r_{bio} is the reaction rate (mol/m^3/s); k is the rate constant (mol/m^2/s); and A is the effective surface area (m^2) or the contact area between SOC and biomass that depends on the amount of biomass as biomass is not explicitly represented. The depth function $f(Z_w)$ accounts for the variable accessibility of SOC along depths and takes the form $f(Z_w) = \exp\left(-\frac{Z_w}{b_m}\right)$, where Z_w is the water table depth (m) and b_m (0.5 m) characterizes the SOC decrease over depth (Hagedorn et al., 2001; Weiler & McDonnell, 2006). The $f(T)$ and $f(S_w)$ describe the rate dependence on soil temperature and moisture, respectively. The $f(T)$ takes the widely used Q_{10}-based form $f(T) = Q_{10}^{|T-20|/10}$, where Q_{10} is the relative increase in reaction rates when temperature increases by 10 °C (Hararuk et al., 2015). Global synthesis shows that Q_{10} generally varies from 1.4 to 2.4 (Liu et al., 2017; Zhou et al., 2009). Here we take a commonly used median value of 2.0. The $f(S_w)$ takes the form of $f(S_w) = (S_w)^n$, where n is the exponent reflecting effects of soil water content on

reaction (Yan et al., 2016); a value of $n = 2$ is considered applicable for most soil textures (Hamamoto et al., 2010).

The simple rate law equation 2 was used for the transformation from SOC to DOC, assuming constant microbe composition and abundant electron acceptor (O_2) and donor (carbon). This captured the DOC dynamics, so we did not use the more complex Monod rate law and explicit microbe representation, which would unnecessarily introduce additional parameters. The code does have the capability of using a more generalized Monod rate law with explicit representation of microbes.

The bio-module BioRT has been verified against the widely used reactive transport model CrunchTope on soil carbon and nitrogen processes, which we do not elaborate here. Although BioRT-Flux-PIHM can be run using a spatially explicit domain, for this work, we used a scheme with two grid blocks, each representing one side of the watershed connected by a river channel (Figure 2). Although the processes included are the same, the spatially implicit scheme has a smaller number of parameters and is computationally less expensive.

3.3 BioRT-Flux-PIHM Setup and Calibration

Flux-PIHM takes in watershed characteristics, initial water conditions, and climate forcings (time series of precipitation and temperature). Watershed characteristics are from National Elevation Dataset (topography), National Land Cover Database, Moderate Resolution Imaging Spectroradiometer (Leaf Area Index), and Soil Survey Geographic Database. Flux-PIHM outputs water storage and water fluxes (e.g., overland flow, infiltration, recharge, subsurface lateral flow, and river flow), which are used in BioRT when solving the reactive transport equation 1 for water chemistry.

The reaction processes were simulated using BioRT-Flux-PIHM for DOC and Na as representatives of flushing and slight dilution C-Q relationships. The reactive solutes, DOC and Na, are involved in multiple reactions (Table 1). DOC is a product of microbe-mediated SOC decomposition where microbes break down large organic carbon compounds into smaller, soluble organic carbon compounds. The reaction rates follow the equation 2 as influenced by SOC and biomass abundance and soil moisture and temperature. The model does not consider details of multiple SOC pools with different reactivities as typically done in the SOC community (Wieder et al., 2013). The goal is to keep the reactions simple such that only necessary parameters are introduced. DOC also complexes with soil clays (Herndon et al., 2017), which can retard DOC and serve as a storage mechanism. Na sources from albite dissolution that follows the Transition State Theory rate law (Table 1). The SOC content was averaged as 2% (v/v) based on soil data from Soil Survey Geographic Database. With the lack of field measurements, the volume fraction of albite was assumed to be 1% based on Woodruff et al. (2015) and Shmakin (1979), where rocks in this area have been shown to contain 0.5–3% albite (roughly 10% feldspar (v/v) with 5–30% being albite).

Table 1
Reactions and Reaction Parameters (From the EQ 3/6 Database (Wolery, 1992) Unless Otherwise Noted)

Reaction network	Rate law	$Log_{10}k$ (mol/m^2/s)	$Log_{10}K_{eq}$	SSA (m^2/g)
Kinetic-controlled reactions				
$SOC \rightarrow DOC$	$kAf(Z_w)f(T)f(S_w)$	-10.0[a]	—	**0.092**[c]
$NaAlSi_3O_8(albite)+4H^+ +4H_2O \leftrightarrow Na^+ + Al^{3+} + 3H_4SiO_{4(aq)}$	$kA\left(1-\frac{IAP}{K_{eq}}\right)$	-12.0[b]	2.76	**1.26**[c]
Surface complexation (at equilibrium)				
$\equiv X + DOC \leftrightarrow \equiv XDOC$		—	**1.10**[c]	—

Note. *IAP* is ion activity product, and $\equiv X$ represents surface site. Surface area A (m^2) is calculated based on specific surface area (SSA, m^2/g), volume fraction (m^3/m^3), and solid density (g/cm^3). Specifically, the volume fraction of soil organic carbon (SOC) and albite is 0.02 and 0.01 m^3/m^3, respectively; solid density of SOC and albite is 0.224 and 2.62 g/cm^3 (Rawls, 1983), respectively.
[a]Estimation from Wang et al. (2015) and Wieder et al. (2014). [b]Brantley et al. (2008). The albite dissolution rate constant k varies between 10^{-13} and 10^{-10} mol/m^2/s with k values around 10^{-12} under pH = 4–5. [c]Calibrated values (bold). Chiou et al. (1990) reported measured SSA of 0.61–0.70 m^2/g for organic-rich Florida peat and soil humic acid, and Rutherford et al. (1992) reported measured SSA of 1–2 m^2/g for SOC, which is higher than the calibrated 0.092 m^2/g. The SSA of feldspars is reported to vary between 1.8 and 3.0 m^2/g (Peckhaus et al., 2016), also higher than the calibrated 1.26 m^2/g. The surface areas of natural materials that are actually reacting are often orders of magnitude lower than the measured absolute surface areas because hydrological conditions are dynamic and not all surface areas are reacting (Heidari et al., 2017; Wen & Li, 2018).

The model was calibrated considering both hydrology (e.g., time series of snowpack and stream flow) and biogeochemistry data (e.g., time series of concentrations of DOC and Na or [DOC] and [Na] in stream). The best fit was determined by the Nash-Sutcliffe efficiency for reproducing both water and concentration data. Hydrology calibration was done by adjusting parameters related to land surface, soil property, and vegetation and groundwater flow. Groundwater flow was estimated based on groundwater chemistry data and iterative calibration between discharge and stream chemistry. The calibrated hydrology parameters are in Table S1. The biogeochemical calibration adjusts specific surface area for SOC and albite dissolution and the equilibrium constant K_{eq} of DOC complexation, whereas rate constants for SOC decomposition and albite dissolution are based on literature values (Table 1).

Sensitivity analyses were performed by varying reaction kinetics and thermodynamic parameters, as well as soil composition (SOC and albite content) and groundwater composition ([DOC] and [Na]). The groundwater contribution to the stream (%) was varied by a factor of 2 from the best fit case. A total of 500 simulations was carried out using randomly sampled soil and water characteristics across the uncertainty range of volume fraction of SOC and albite (0.1% to 10%) and groundwater [DOC] and [Na] (0.1 to 10 mg/l).

4 Results

4.1 Hydrology

4.1.1 Key Hydrology Parameters

The model generally captures the dynamics of snowpack accumulation in winter and snowmelt in spring, indicating good model-data agreement (Figure 3, daily Nash-Sutcliffe efficiency > 0.90). The model slightly underestimates the snowpack in February and March, possibly due to excessive sublimation and early onset of snowmelt in the Colorado Rocky Mountains (Barlage et al., 2010), processes not well represented in the Noah

Land Surface Model in Flux-PIHM. The most sensitive parameter is C_{zil} (Table S1) for the surface exchange of heat and momentum (Chen & Zhang, 2009). A low C_{zil} (<0.1) leads to high surface skin temperature, large snow sublimation, and early snowmelt, ultimately underestimating snowpack and SWE. It also regulates the timing and magnitude of the discharge peak because snow is the ultimate source of discharge. Low C_{zil} (<0.1) values result in lower and earlier predicted discharge peaks than observations.

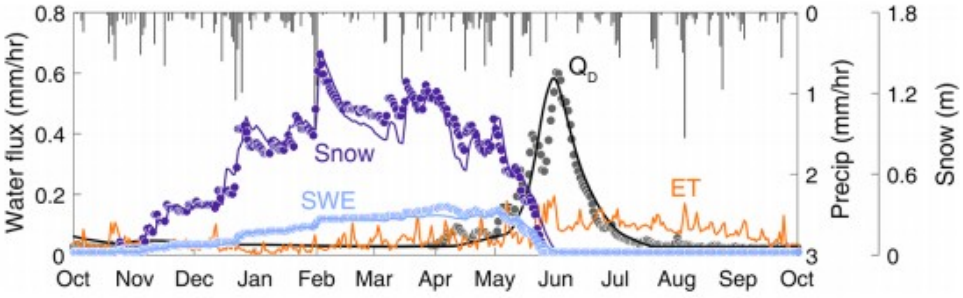

Figure 3. Mountain hydrology and water flux in 2016: snowpack and snow water equivalent (SWE), precipitation (top bar), discharge (Q_D), and evapotranspiration (ET). SWE = snowpack × snow density. Data are filled circles, and model outputs are lines. Water fluxes are normalized by drainage area, 1 mm/hr = 14.7 m^3/s.

The most important soil parameters are the porosity θ and soil thickness Z_{soil} that define the "total storage" (Table S1). Large water storage results in a wide but low discharge peak as it takes more water to saturate the soil with a large water buffering capacity. A large saturated hydraulic conductivity K_{satV} leads to rapid recharge of infiltrated water and early arrival of a large discharge peak. The van Genuchten parameters α and n primarily control soil water retention. Coarser materials (e.g., sand) that readily lose water have larger values and quickly drains water.

4.1.2 Water Dynamics

Figure 3 shows snowpack accumulation that started in November, peaked to over 1.5 m in early February, and melted in the spring. The SWE generally followed the trend of snowpack yet peaked in April instead of February. Considerable snowmelt in April triggered an early peak, followed by massive snowmelt and increasing streamflow until June. Discharge peaked in early June, after which it returned to base flow between August and December.

The model estimates a runoff ratio of 0.50, meaning half of the precipitation is discharged into the stream. The annual ET is estimated to be 0.52 m, similar to the estimated value of 0.42 (±0.06) m for the nearby Deer Creek watershed, Colorado (Claassen & Halm, 1996). Their calculation indicated annual ET varies between 0.23 and 1.0 m with an average of 0.45 (±0.19) m for 18 Rocky Mountain watersheds varying in size, land cover, elevation, and precipitation. Daily ET in the warm and wet periods (May to September) averages at 0.083 (±0.038) mm/hr, about 2.4 times of the ET (0.035 ±

0.022) mm/hr in the cold period from October to April. The warm and cold periods contribute 69% and 31% to the annual ET, respectively.

The discharge (Q_D) consists of three components: the seasonally dynamic surface runoff (Q_S), soil lateral interflow (Q_L), and constant shallow groundwater (Q_G) that do not respond much to the temporal dynamics of surface hydrological conditions. Although not shown here, annual Q_s (0.0014 m) is <1% of the annual discharge (0.50 m), while annual Q_L (0.40 m) contributes 80% to annual Q_D. The calibrated Q_G is 0.011 mm/hr approximating 20% (0.10 m) of the annual Q_D; it is about 5% and 80–95% of Q_D at the snowmelt peak and during the dry time, respectively. The annual 20% contribution to Q_D is consistent with a reported range of 20% to 80% (Beck et al., 2013; Miller et al., 2014). Rumsey et al. (2015) used conductivity mass balance hydrograph separation for 239 diverse sites across the Upper Colorado River Basin and showed approximately 50% of streamflow stems from groundwater discharge.

4.2 Stream Chemistry and Contrasting C-Q Patterns

4.2.1 Temporal Evolution and Contrasting C-Q Relationships

Stream chemistry demonstrates strong seasonal dynamics: DOC remains at low concentrations under base flow and reaches a maximum of ~5 mg/L during snowmelt (Figure 4). Geogenic cations exhibit high concentrations under base flow and low concentrations at high flow, demonstrating a dilution pattern that is opposite of the DOC pattern. Trace metals reach their maxima at early flushes before the discharge peak and remain low afterward. BioRT-Flux-PIHM reproduces the timing and magnitude of major peaks for DOC and Na, although some small fluctuations escape the model simulation. The model also shows consistent underestimation in the low flow period.

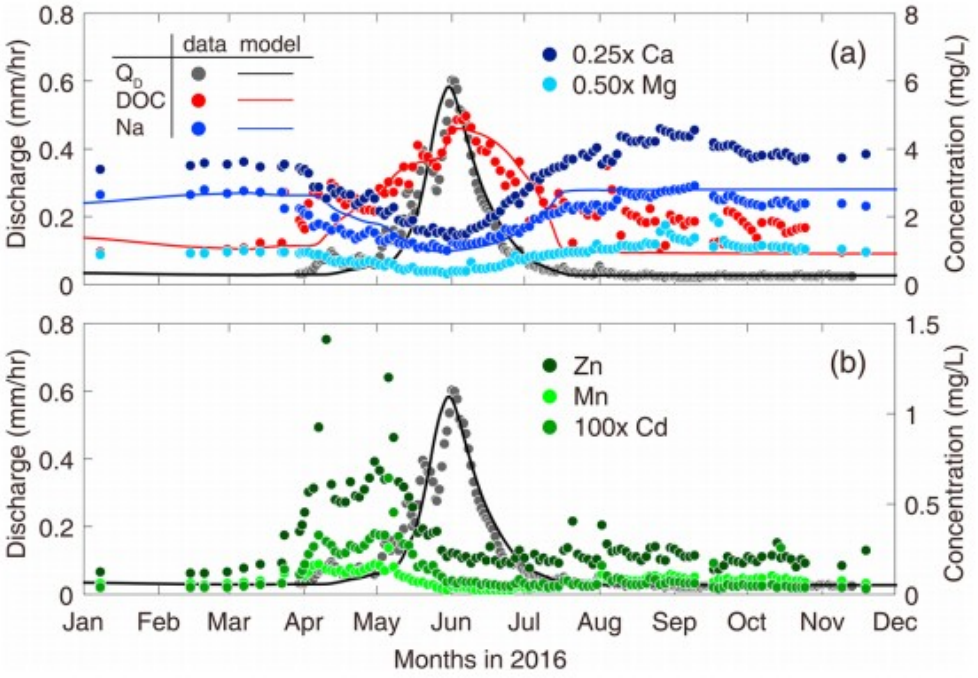

Figure 4. Time series of stream chemistry: (a) biogenic species (DOC) and geogenic species (Na, Ca, and Mg); (b) trace metals (Zn, Mn, and Cd). Ca, Mg, and Cd are plotted as 0.25 (0.25×), 0.5 (0.5×), and 100 (100×) times of their measured concentrations, respectively, such that all solutes show up clearly in the plotted concentration range. DOC = dissolved organic carbon.

Biogenic solutes (i.e., DOC, TN, TON, and DTN) exhibit flushing C-Q patterns, whereas Ca, Na, Mg, and Cl show dilution patterns (Figure 5). Although LFM and HFM data were collected at different times and frequency, they show relatively consistent dynamics. The model reproduces C-Q relationships of DOC and Na. Trace metals mirror DOC in early snowmelt stage and reached their maxima at medium flow but decrease under high flow conditions. The relatively linear increase in DOC and nitrogen concentrations indicate transport-limited conditions, while clockwise hysteresis patterns of trace metals indicate supply-limited conditions (Duncan et al., 2017; Zarnetske et al., 2018). The early flush potentially suggests the accumulation of metals and/or the formation of DOC-metal complexes. Metal-DOC complexation is well-documented and has been reported to enhance metal mobility and reduce metal sorption on soil (Neagoe et al., 2012). The decreases of trace metal concentrations under high flow conditions could be attributed to small soil stores and quick depletion due to either limited metal-containing zones or slow dissolution rates (Nagorski et al., 2003; Roussiez et al., 2013). Stream Cd occasionally exceeds the Environmental Protection Agency (EPA) Maximum Contaminant Level (MCL) of 0.005 mg/L, whereas Mn exceeds the EPA's Secondary MCL (SMCL) of 0.05 mg/L for more than half of the measurements. These data accentuate the value of high-frequency data: Although LFM data show similar concentration levels and trends, only the HFM captures the complete cycle of the hysteretic loop during snowmelt.

Total export fluxes, or daily load (mass/d), of the solutes estimated using the USGS Load Estimator (Runkel et al., 2004) show that discharge from May to July accounts for nearly 80% of the annual discharge. In this period, 90% of annual DOC export occurs, compared to 70% and 75% for geogenic solutes and trace metals, respectively. In essence, spring melt is the hot moment that exports disproportionally large amount of solutes (70–90%; Raymond & Saiers, 2010).

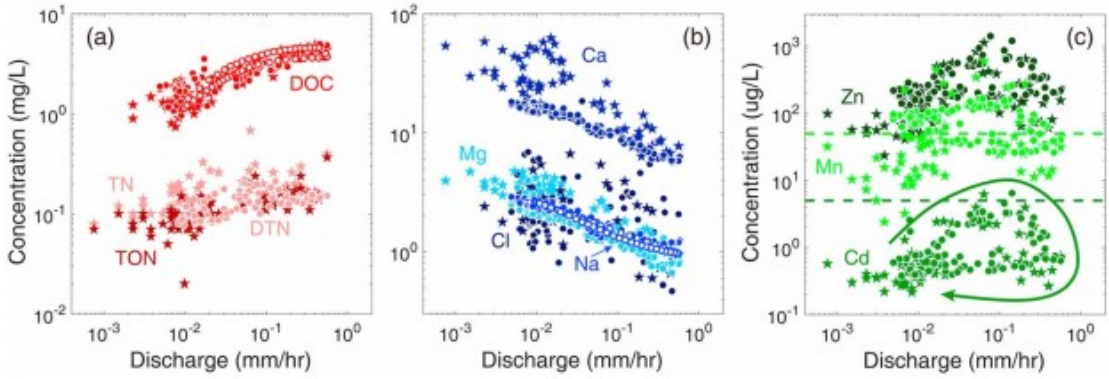

Figure 5. Concentration-discharge relationships: (a) flushing behavior of DOC (slope $b = 0.23$), TN ($b = 0.12$), TON ($b = 0.19$), and DTN ($b = 0.12$); (b) dilution behavior of Na ($b = -0.22$), Ca ($b = -0.24$), Mg ($b = -0.27$), and Cl ($b = -0.11$); and (c) clockwise hysteresis loops of metals. Filled circles and stars represent high-frequency measurement in 2016 and long-term low-frequency measurement data (2007-2016), respectively. Open circles (DOC and Na) are model output. The dashed lines are Environmental Protection Agency (EPA) Maximum Contaminant Level for Cd and Secondary Maximum Contaminant Level for Mn. DOC = dissolved organic carbon; TN = total unfiltered nitrogen; TON = total unfiltered organic nitrogen.

4.2.2 Concentrations Versus Rising Water Table

Various studies have suggested that elevated biogenic concentrations (e.g., DOC and N) at high flow can be caused by rising water table flushing organic-rich shallow soil water (Creed et al., 1996; Seibert et al., 2009). Figure 6 illustrates the model output that indicates such dynamics. As the water table depth (depth to the ground surface) rises from −2.7 to −1.4 m, [DOC] increases, whereas [Na] decreases. The rising limb of the [DOC] increases as the rising water table taps sorbed DOC and also continues to decompose SOC. As the water table rises further and flushes more organic rich water, [DOC] increases even further. Sensitivity analysis indicates (not shown here) that the $f(z_w)$ term in equation 2, that is, the depth dependence of rates that lead to high rates in the shallower zone with higher SOC content, determines the hysteresis. This echoes other studies that attributed counterclockwise C-Q to delayed transport (Bowes et al., 2009; Tunaley et al., 2016). In our case, the DOC transport from shallow soils with abundant SOC is delayed because the water table has to rise higher to do so. In contrast, groundwater has higher [Na] than shallow waters, such that the rising water with cation-poor shallow soil water dilutes Na in the stream.

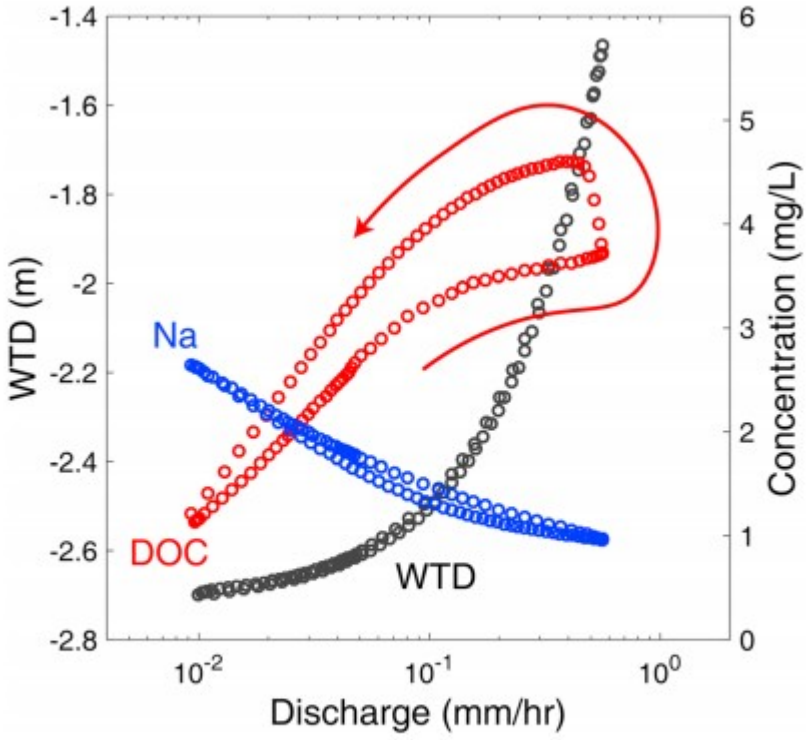

Figure 6. Modeled WTD and [DOC] and [Na] versus discharge. DOC = dissolved organic carbon; WTD = water table depth.

4.2.3 End-Member Source Waters

Stream water is derived primarily from three sources with distinct chemistry: surface runoff Q_s that resembles rainwater, upper soil water lateral flow Q_L with enriched organic species but relatively low cations (yet can be highly variable), and shallow groundwater Q_G from connected aquifers with high concentrations of cations as weathering products (Li, Bao, et al., 2017). Figure 7a shows that concentrations of DOC and metals are higher in stream water and those of geogenic solutes and Cl are higher in groundwater. The geogenic species source from mineral weathering upon long-time contact between water and rocks. The National Atmospheric Deposition Program rainwater data (site ID: CO10, 1999–2016) show that average concentrations of Ca, Na, Mg, and Cl in rainfall are about one to two orders lower than those in groundwater. Figure 7b shows [DOC] and [Na] in end-members waters. Groundwater [DOC] was from a shallow groundwater at a nearby Deer Creek watershed (CO) and showed a steady [DOC] of approximately 1.1 mg/L under low flow conditions (Boyer et al., 1997). Groundwater [Na] was inferred from a local well. Although there are three end-members, surface runoff has a negligible contribution to the stream (<1% annually) and has negligible impact. The stream chemistry slides between soil water and groundwater, approaching soil water composition under wet conditions when soil water dominates discharge. Under dry conditions, groundwater is predominant

such that the stream composition shifts toward the groundwater chemistry. This indicates that contrasting trends of DOC and Na are caused by seasonally variable dominance of source waters and their distinct water chemistries.

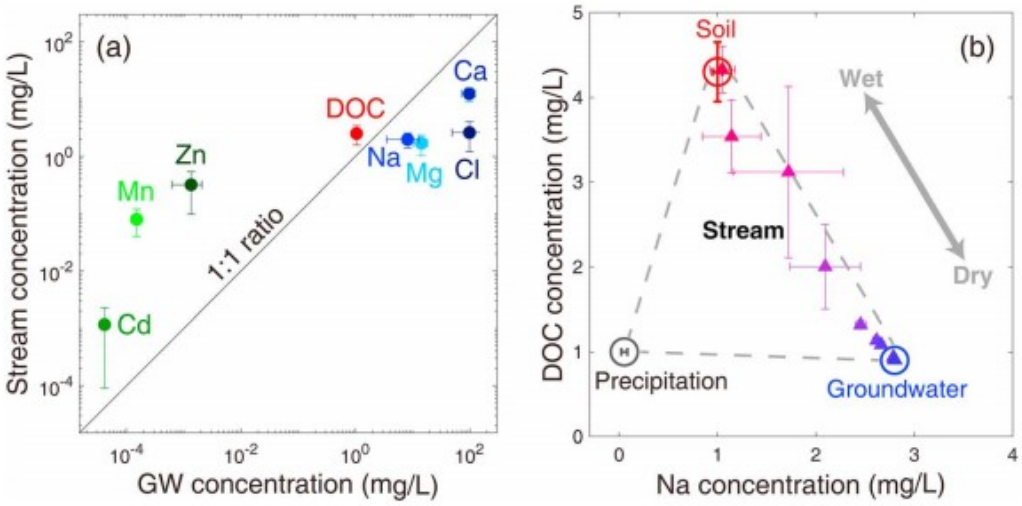

Figure 7. (a) Measured stream versus groundwater chemistry. (b) End member water chemistry of DOC and Na (circles) and monthly averaged stream chemistry (triangles). Error bars are for one standard deviation. Some error bars are smaller than symbol size and are invisible. Stream chemistry mostly slides between soil water (wet condition during snowmelt) and groundwater (dry condition). Precipitation has negligible impacts because of the small contribution of surface runoff to the stream (<1% annually). DOC = dissolved organic carbon.

4.3 Controls of C-Q Relationships

4.3.1 Reaction Kinetics and Thermodynamics

As has been shown previously, C-Q relationships depend on the relative contribution and composition of end-member source waters, both of which vary with climate, land cover, and geological conditions (Schwab et al., 2017; Woodruff et al., 2015). Figure 8 shows a sensitivity analysis with varying decomposition rate constant k and DOC sorption coefficient K_{eq}. Note that varying k has a similar effect as varying SOC surface area (changing volume fraction), as they are multiplied in equation 2. Specifically, higher rates of SOC decomposition (2k, two times higher) elevate [DOC] in soil water and eventually lead to a more pronounced flushing pattern. In addition, stronger sorption with larger K_{eq} (10×) of DOC complexation on soil surface (Table 1) maintains relatively constant, low [DOC] and chemostatic behavior; weaker sorption with lower K_{eq} (0.1×) leads to higher [DOC]s and flushing patterns (Figure 8c). Note that both reaction kinetics and sorption equilibrium do not change the timing of [DOC] peak, indicating the timing is primarily controlled by hydrological processes instead of reaction characteristics. Similarly, higher albite dissolution rates (2×) lead to a more subdued dilution pattern as the soil water elevates to a level closer to the groundwater (Figure 8e). For Na, the equilibrium constant K_{eq} (e.g., mineral solubility; Table 1) barely influences stream concentration and C-Q patterns (Figure 8f), because albite

dissolution rarely reaches equilibrium. These trends indicate that the same solute can have flushing or dilution patterns, depending on the concentration differences in shallow soil water and deeper groundwater.

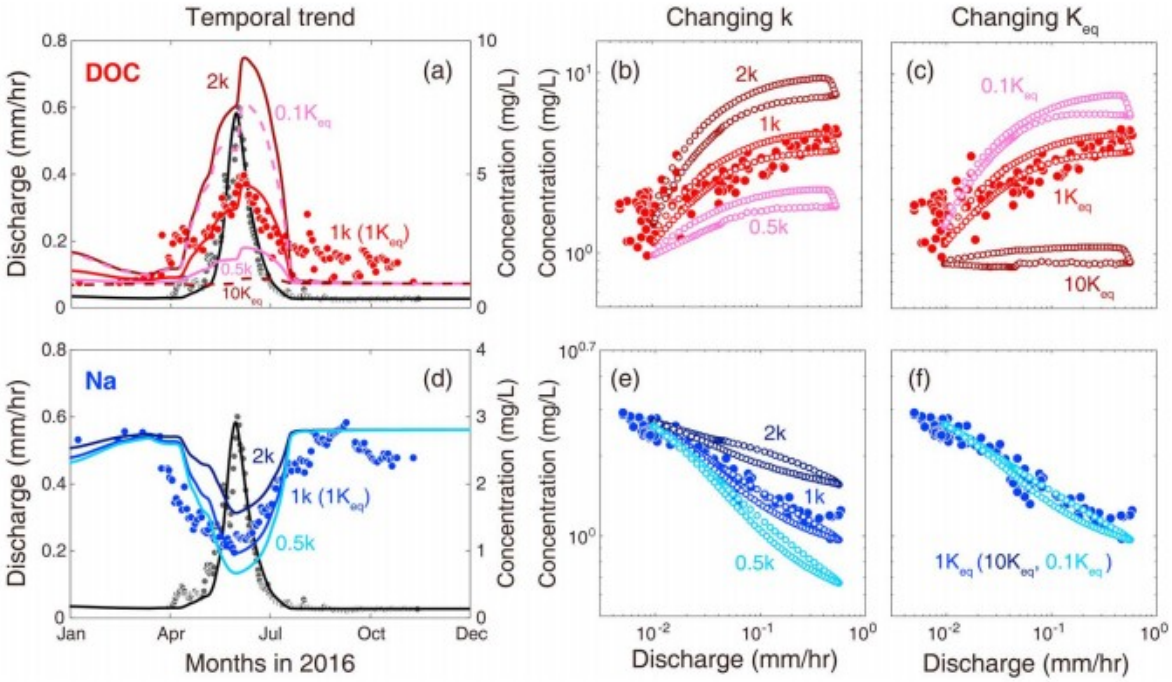

Figure 8. Sensitivity analysis for identifying controls of DOC and Na reaction kinetics k (rate constant) and thermodynamics K_{eq} (equilibrium constant). (a)–(c) is DOC, and (d)–(f) is Na. "1k (Keq)" is the calibrated base case, whereas the "2k" case doubles the rate constant while keeping all other parameters the same as the base case. The first column (a) and (d) is the temporal trend, and the second and third columns are concentration-discharge figures when using different k and K_{eq}. Filled circles are data; lines and open circles are model results. For Na, cases with different K_{eq} overlap because the system is not limited by reaction thermodynamics. DOC = dissolved organic carbon.

4.3.2 Groundwater Chemistry and Quantity

Figure 9 suggests that changing groundwater chemistry can have large impacts on C-Q patterns (Figures 9a and 9c) with an effect that is similar to changing soil water composition via reaction kinetics and thermodynamics in Figure 8. In contrast, varying groundwater volume contribution to the stream only slightly alters C-Q patterns (Figures 9b and 9d). In cases with "no groundwater," chemostasis occurs because soil water as a single end-member does not lead to sufficient concentration gradients to change C-Q patterns. This indicates that the presence of groundwater is essential in determining C-Q patterns.

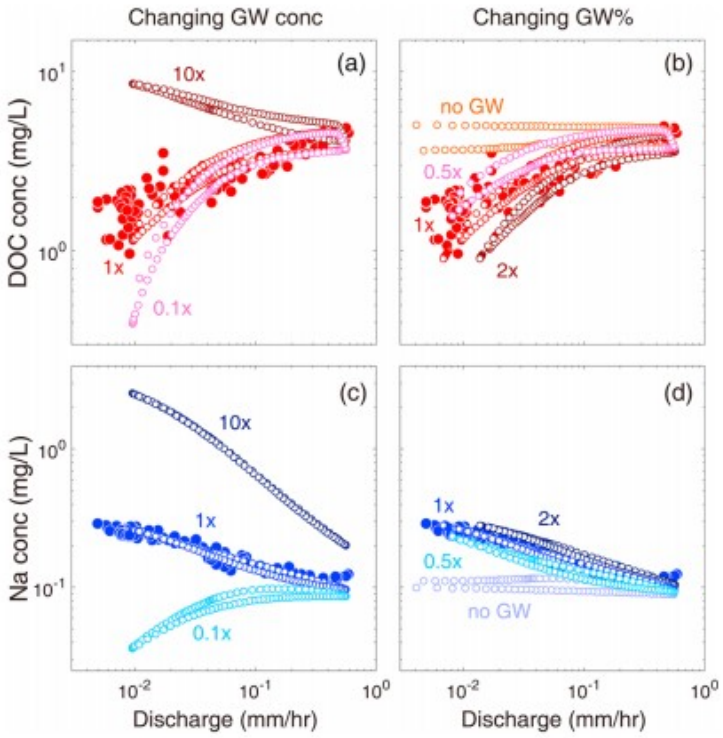

Figure 9. Sensitivity analysis for identifying key controls of groundwater composition (left) and volume input (right). The changing composition has higher impacts than changing volume input to the stream. Cases without groundwater input lead to chemostatic behaviors. DOC = dissolved organic carbon.

4.3.3 A General Relationship Between C-Q Slope *b* and End-Member Concentration Ratio C_{ratio}

The Monte-Carlo simulation of 500 runs sampled across the uncertainty range of SOC and albite (0.1% to 10%), and groundwater DOC and [Na] (0.1 to 10 mg/L) show large variations in soil water and groundwater concentrations (Figure 10). Each circle in the figure represents one run with corresponding constant groundwater concentrations and soil water concentration calculated as volume-weighted averages across the whole year. The cluster pattern shows that flushing patterns ($b > 0.1$) cluster toward the upper left with high soil water concentrations (C_{sw}) relative to groundwater concentrations (C_{gw}). In contrast, dilution ($b < -0.1$) occurs toward the bottom right with high C_{gw} relative to C_{sw}. Chemostasis shows up close to the 1:1 line, as long as the soil and groundwater concentrations are similar with a concentration ratio ($C_{ratio} = C_{sw}/C_{gw}$) between 0.6 and 1.8.

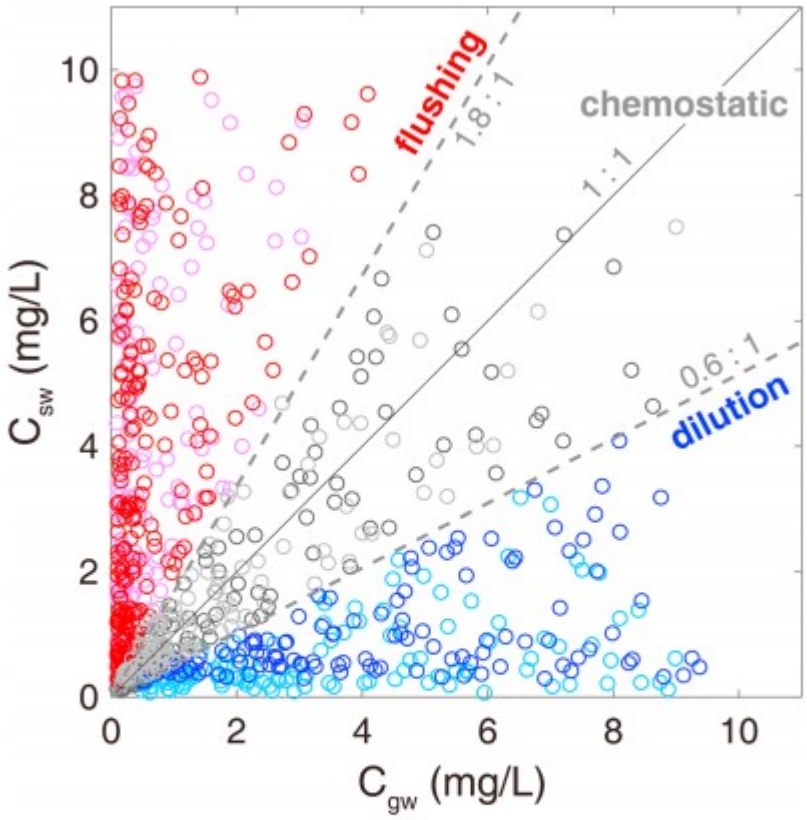

Figure 10. Cluster pattern of dissolved organic carbon and Na soil water and groundwater concentrations from 500 Monte-Carlo simulation cases. Each open circle represents the average soil and groundwater concentrations of dissolved organic carbon (light color) or Na (dark color) in one of the 500 runs. The two gray dashed lines are the thresholds separating flushing (red color, $b > 0.1$) and dilution (blue color, $b < 0.1$) patterns from chemostatic (gray color, $-0.1 < b < 0.1$) patterns.

Plotting C-Q slope b against C_{ratio} in all cases, these values collapse onto a curve (Figure 11), with flushing patterns ($b > 0.1$) at $C_{ratio} > 1.8$ and dilution pattern ($b < -0.1$) at $C_{ratio} < 0.6$, and chemostasis in between. Although the threshold C_{ratio} values can be system specific, the curve follows the relationship:

$$b = \frac{\delta_b \, C_{ratio}}{C_{ratio,1/2} + C_{ratio}} + b_{min}, \quad (3)$$

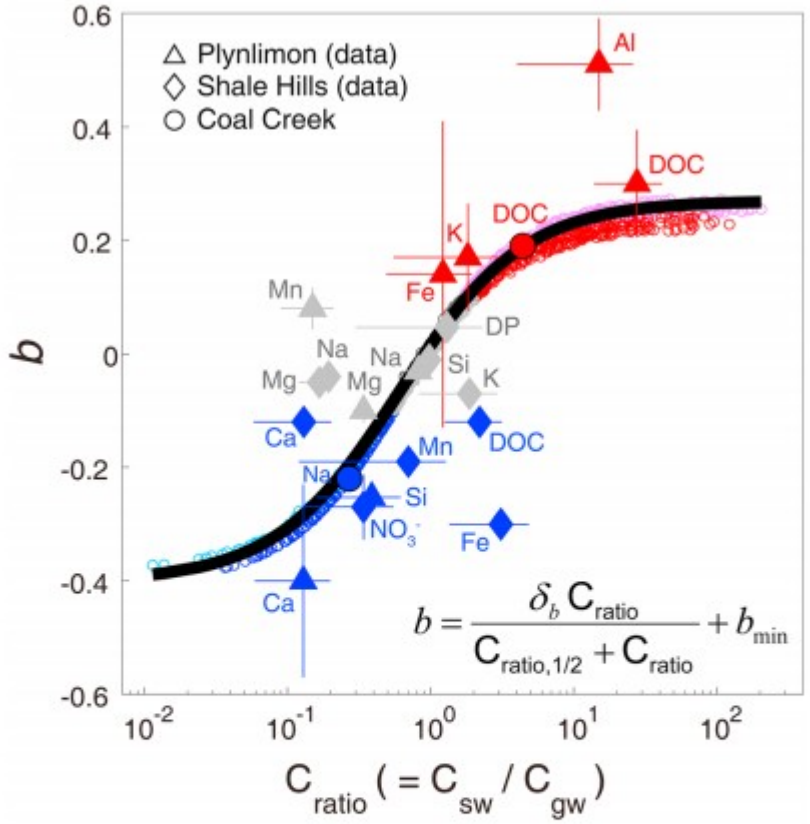

Figure 11. Concentration-discharge slope b as a function of concentration ratio ($C_{ratio} = C_{sw}/C_{gw}$). Overlapped open circles constituting the curve are from 500 Monte-Carlo simulation cases (DOC in light color and Na in dark color). The black line is the equation (3) in the figure. Here $\delta_b = 0.67$, $C_{ratio,1/2} = 0.61$, and $b_{min} = -0.40$. Also plotted are b and C_{ratio} with error bar (one standard deviation) calculated from measurements from three watersheds (Coal Creek, Shale Hills, and Plynlimon). DP is dissolved phosphorus. DOC = dissolved organic carbon.

where δ_b is the difference between maximum b (b_{max}) and minimum b (b_{min}), and $C_{ratio,1/2}$ is the concentration ratio when b = ½ (b_{max} + b_{min}). In this work, b_{max} = 0.27 and b_{min} = −0.40, so that δ_b = 0.67. The value of $C_{ratio,1/2}$ is 0.61 corresponding to a b value of −0.07. The b_{max} and b_{min} determine the upper and lower limits of b values, and $C_{ratio,1/2}$ determines the shape of the curve. The limits of the curve are likely determined by the thermodynamic and kinetic characteristics of DOC and Na reactions, as will be discussed later.

Figure 11 also shows C-Q slope b and C_{ratio} values compiled from two other catchments: Shale Hills in Pennsylvania and Plynlimon in Wales, UK (Herndon et al., 2015a). In general, we see that data points follow the curve defined by equation 3, although the range of b values may vary for different catchments and solutes. Notice again that the same solute can have different C-Q patterns and different solutes can have the same C-Q patterns in different

catchments. DOC shows flushing in Plynlimon and slight dilution in Shale Hills. Potassium (K) shows flushing in Plynlimon and chemostasis in Shale Hills. Si exhibits chemostasis in Plynlimon and slight dilution in Shale Hills. In both Shale Hills and Plynlimon, C_{ratio} values calculated from measurements are within the modeled range for Coal Creek. Fe and Mn at Shale Hills exhibit higher C_{ratio} than other species (e.g., Ca and Si) that exhibit dilution, possibly because they complex with DOC, resulting in enriched soil water and thus higher C_{ratio} (Herndon et al., 2015a). Plynlimon has a wider range of slope *b* (e.g., Al, DOC, Fe, and Ca) than the modeled range of −0.40 and 0.27 at Coal Creek, which could be attributed to their specific hydrologic differences.

5 Discussion

5.1 The Conceptual Model

A conceptual model (Figure 12) illustrates the interplay between subsurface biogeochemical heterogeneity of the solute sources and temporal variability of predominant flow in shaping the C-Q patterns. Specifically, the hillslope view shows the predominance of groundwater under dry conditions and soil water under wet (snowmelt) conditions in stream water. Solutes that are enriched in shallow soil (red triangle in top left in Figure 12) result in high C_{ratio} that lead to a flushing pattern; solutes that are abundant in deeper groundwater (blue triangle in top left) are diluted by shallow soil water under high flow conditions. Generally, biogenic species are abundant in shallow soils as they reflect the signature of life. Sources of geogenic solutes, mostly unweathered or less weathered rock, are often ample at depth.

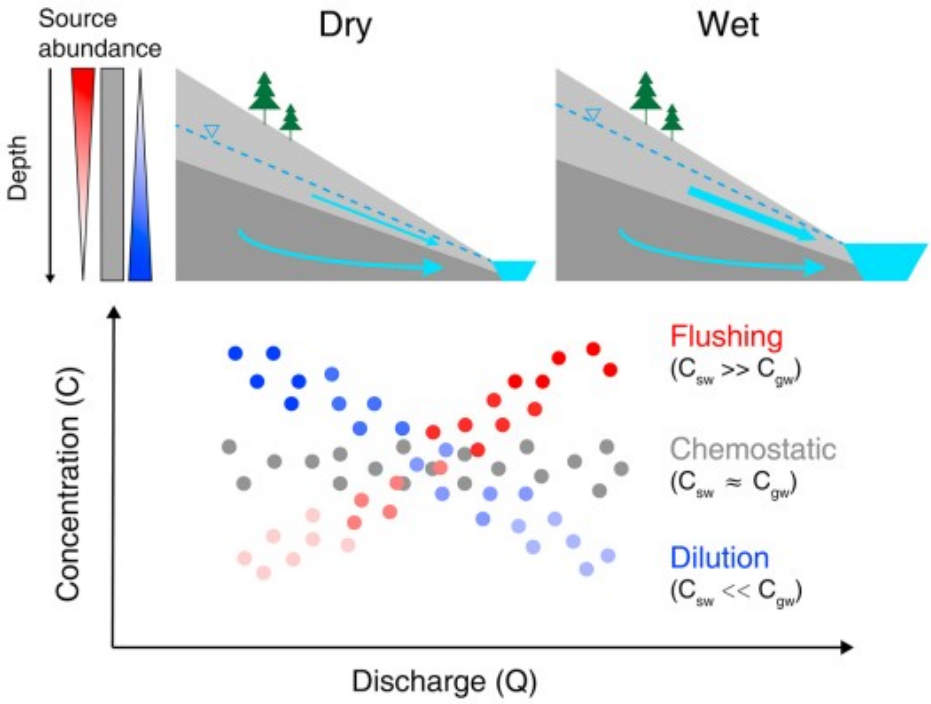

Figure 12. A schematic diagram about mechanisms leading to different C-Q patterns. The top left panel indicates the subsurface biogeochemical heterogeneity or spatial patterns of solute source materials along depths that lead to concentration contrast, which eventually results in flushing (red), chemostatic (gray), and dilution (blue) C-Q patterns. The hillslope view shows the predominance of groundwater under dry conditions and soil water under wet (snowmelt) conditions in stream water. The combination of the source chemistry spatial heterogeneity and the switch in source water predominance leads to different C-Q patterns. C-Q = concentration-discharge.

Boyer et al. (1997) showed a significant [DOC] difference between upper soil (7–46 mg/L) and shallow groundwater (1–8 mg/L) in Deer Creek, CO. Hornberger et al. (1994) and Boyer et al. (1996) concluded that the key to reproduce a flushing pattern is to constrain a two-reservoir model with the deeper soil reservoir with a lower constant [DOC] (1.2 mg/L) and the upper soil reservoir with a much higher [DOC] (5– 35 mg/L), which is in line with our conceptual figure here. Such hypotheses have also been illustrated to explain the flushing behavior of N (Creed et al., 1996; Weiler & McDonnell, 2006), as well as contrasting C-Q behaviors of different solutes (Bishop et al., 2004). These ideas are based on relatively simple conceptual models, and they convey a very similar message as what we have here with complex, process-based hydrological and biogeochemical process representation. This indicates that the first-order dynamics can be delineated by representing watersheds with shallow and deep compartments and their essential biogeochemical gradients along depths.

Equation 3 (and Figure 11) says that C-Q slopes are determined by concentration contrasts between end-member source waters under different flow regimes. The end-members are the groundwater as the base flow under dry times and soil water at high flow. If the end-member water compositions

are not “sufficiently” different, chemostasis occurs, as has been widely observed for many geogenic species (Godsey et al., 2009). This may be because of prevalent sources of geogenic species in many geochemical settings. They can dissolve out from clays in weathered shallow soils and from minerals in unweathered rocks at depth. The concentrations in the shallow soil and groundwater may be different but not sufficiently different to allow for the emergence of chemodynamic behavior. Li, Bao et al. (2017) hypothesized that chemostatic behavior of Cl and Mg arises from synchronized changes in dissolution rates and flow with “wetted” mineral surface areas being the key connection of the two. In that case, C_{ratio} of Cl and Mg were 0.57 and 0.43, respectively, such that the concentration differences in soil and groundwater are relatively small. When the dissolution rates were set to lower values in a sensitivity analysis leading to a lower C_{sw} and lower C_{ratio} of 0.23, dilution did occur, which is consistent with the conclusions drawn here. Soil water compositions are commonly measured because they are more accessible than groundwater. Although groundwater has long been recognized as a critical component of the water balance (Gurdak, 2017; Taylor et al., 2013), its comparative inaccessibility results in much more scarce data sets. This work highlights the importance of measuring groundwater chemistry and indicates that they may be inferred from stream chemistry at low flow conditions.

5.2 What Determines Thresholds and Limits?

A natural next question is what determines parameters (b_{min}, b_{max}, and $C_{ratio,1/2}$) in equation 3? The sensitivity analysis (Figure 8) indicates that reaction kinetics and thermodynamics can play a key role in determining end-member concentrations. They allude to the fact that reaction characteristics that amplify concentration contrasts between shallow and deep zones and lead to more pronounced flushing or dilution behavior. This echoes recent findings (Ameli et al., 2017) at the hillslope scale that minerals with high ratios of equilibrium concentration versus intrinsic weathering rate lead to dilution C-Q patterns because more concentration contrasts can develop between shallow and deep zones, whereas smaller ratios drive the system toward chemostasis due to low mineral solubility (low equilibrium concentrations) and relatively similar concentrations in shallow and deep zones). This may explain why TN shows mostly flushing patterns in agriculture lands (Basu et al., 2010; Thompson et al., 2011). The dominant form of TN in agricultural land, nitrate (NO_3^-), is very soluble and dissolves very fast in top soils with heavy fertilizer addition such that its concentration is often high in shallow soil, leading to high C_{ratio}. TP also mostly shows flushing behavior in agriculture lands (King et al., 2015; Vanni et al., 2001). This is because P is barely soluble, so TP is dominated by particulate P (PP) sorbed on fine particles that are mobilized at higher discharge, leading to higher PP in shallow zones. In other words, reaction characteristics that amplify the concentration contrasts lead to more dynamic C-Q patterns. Note

that BioRT-Flux-PIHM can be applied to model TP and/or PP by adding a sediment species that can complex with dissolved phosphorus.

Chemical and reaction difference alone cannot explain all behavior: NO_3^- has been observed to exhibit all three C-Q patterns (Abbott et al., 2018; Miller et al., 2016). The extent of concentration contrasts in shallow soil and groundwater zones also depends upon the subsurface structure and extent of connectedness in different zones (e.g., the presence of fractures; Hyer et al., 2016). A sharp interface often exists between shallow soil and weathered regolith with high permeability and porosity contrasts (Welch & Allen, 2014). More fractured regolith enables vertical flow from the shallow zone into deeper reservoirs, thereby increasing the connectedness and alleviating the differences between shallow and deep zones. Generally, lower permeability contrasts between reactive and nonreactive zones enhance the similarity of water chemistry (Wen & Li, 2017, 2018; Wen et al., 2016). Musolff et al. (2017) represented catchment structural heterogeneity as mobile and immobile zones and analyzed several solutes in over 61 catchments. Their work indicates that weak correlations between structural heterogeneity and travel time, or relative similar concentration distributions, lead to chemostasis, whereas strong heterogeneity-travel time correlations lead to more dynamic C-Qs (dilution or flushing). Future work should be directed to understand the variables that determine these parameters in equation 3.

5.3 End-Member Source Waters in the Horizontal Direction

Although different C-Q patterns in Coal Creek are caused by concentration contrasts in the vertical direction (shallow vs. deep), equation 3 can also be applied for source zone heterogeneity in the horizontal direction (e.g., valley/riparian zone vs. uphill). For example, Shale Hills has enriched SOC in swales that persistently contribute flow even under dry conditions and low SOC in planar slopes and uplands that are only tapped at high discharge (Andrews et al., 2011). As a result, their C-Q shows slight dilution for DOC. In contrast, Upper Hafren in Plynlimon has abundant SOC and DOC in upland peats, where organic-rich water only connects to the stream during high discharge conditions when the water tables rises sufficiently (Herndon et al., 2015a), which aligns well with the analysis here. Similarly, Sullivan et al. (2018) found that stronger landscape heterogeneity in headwater catchments shows a greater degree of chemodynamic behavior for most geogenic species than downstream watersheds.

5.4 Trace Metals and C-Q Hysteresis

Trace metals have been shown in the literature to form complexes with DOC and flush out at high flow. In the seasonally snow-covered Loch Vale watershed (CO), 4 years of stream chemistry data shows that organic complexation was likely responsible for the spring flush of trace metals and rare earth elements (e.g., Se and La; Shiller, 2010). Trostle et al. (2016) indicated that DOC complexation and colloidal transport influenced C-Q of trace metals (e.g., Cu, Mn, and Ti) in Marshall Gulch watershed. McIntosh et

al. (2017) also attributed the positive C-Q relationships of Ge, Al, and Mn to DOC complexation in the La Jara catchment.

Trace metals exhibit hysteresis that differs from DOC and Na. The early flush occurs on the rising limb (Figure 5), suggesting that significant portions of snowmelt routed through shallow organic-rich soils that are close to mine-impacted areas (Sphagnum bog at Iron Fen), mobilizing metals as organic-metal complexes accumulated during pre-event months. It is possible that as flow continues to increase, the reservoir of complexed metals is exhausted or meltwater reaches outside of mine-impacted areas with negligible trace metals such that metal concentrations decrease at high discharge. This indicates a potentially limited source of metal-containing zones (Nagorski et al., 2003; Roussiez et al., 2013) and/or possible slow dissolution rates that limit metal liberation. In fact, a larger hysteretic loop has been shown to indicate small storage and thus quick depletion during water flushing (Bowes et al., 2005). We rarely observed a large hysteresis loop in the 500 runs, indicating that the homogeneous representation of the watershed with the simple model (two cells + one river) may not capture such dynamics without explicit spatial representation of heterogeneity.

6 Conclusions

Understanding concentration-discharge relationships is essential for illuminating processes that govern chemical weathering and biogeochemical cycling at the watershed scale. This work tests the hypothesis that contrasting C-Q patterns are shaped by switching predominance of end-member source waters in the stream under transient hydrological conditions and their water chemistry contrasts arising from subsurface biogeochemical heterogeneity. We use data from Coal Creek, a snow-dominated high elevation mountainous watershed in Colorado, and process-based reactive transport modeling (BioRT-Flu(x-PIHM). We show that as stream water shifts from groundwater-dominant under dry conditions to soil water-dominant under wet conditions. Concentrations of solutes (e.g., DOC and nutrients) that are abundant in shallow soils continue to increase as the water table rises and taps the organic-rich soil water, exhibiting flushing patterns. In contrast, for geogenic species (e.g., Na, Ca, and Mg) that are abundant at depth, the cation-rich groundwater that dominates the stream under dry conditions becomes diluted by the surging of cation-poor soil water during snowmelt, resulting in the dilution C-Q pattern. Chemostasis occurs when solutes have relatively similar soil water and groundwater concentration levels. These combinations are encapsulated in a general relationship between slope b and soil versus groundwater concentrations ($C_{ratio} = C_{sw}/C_{gw}$): $b = \frac{\delta_b C_{ratio}}{C_{ratio,1/2}+C_{ratio}} + b_{min}$, where δ_b is the difference between maximum b (b_{max}) and minimum b (b_{min}), and $C_{ratio,1/2}$ is the concentration ratio when b = ½ (b_{max} + b_{min}). In Coal Creek, b_{max} = 0.27, b_{min} = −0.40, δ_b = 0.67, and $C_{ratio,1/2}$ = 0.61. At C_{ratio} < 0.6, dilution occurs; at C_{ratio} > 1.8, flushing occurs; chemostasis happens in between. Disparate C-Q patterns of 11 different solutes (DOC,

dissolved phosphorus, NO_3^-, K, Si, Ca, Mg, Na, Al, Mn, and Fe) from three watersheds (i.e., Coal Creek, Shale Hills, and Plynlimon) under varying climate and geologic conditions follow this equation. This indicates the essential role of shallow-deep biogeochemistry contrasts and the corresponding water chemistry in shaping C-Q. The equation may promise broad applications for quantifying and predicting C-Q patterns for a wide range of solutes in watersheds of diverse characteristics, although the parameters in the equation may vary depending on specific conditions.

Acknowledgments

We acknowledge Editor Jean Bahr, the Associate Editor, and three anonymous reviewers for their constructive and thoughtful reviews. This study was supported by the U.S. Department of Energy (DOE) Subsurface Biogeochemical Research (SBR) program (DE-SC0016221). Additional funding is from the Watershed Function Science Focus Area at Lawrence Berkeley National Laboratory funded by the DOE SBR under the contract DE-AC02-05CH11231. We thank Ashley Bembenek and the Coal Creek Watershed Coalition (CCWC) for their water data support. All data are available at data portal for East River watershed in Colorado, managed by Lawrence Berkeley National Laboratory. The original code BioRT-Flux-PIHM is available on the GitHub website (https://github.com/PSUmodeling/BioRT-Flux-PIHM). This website is developing, with detailed instructions and example files added over time. A model development manuscript is in preparation, to be published with information on code structure and application examples.

References

Abbott, B. W., Moatar, F., Gauthier, O., Fovet, O., Antoine, V., & Ragueneau, O. (2018). Trends and seasonality of river nutrients in agricultural catchments: 18 years of weekly citizen science in France. *Science of the Total Environment*, 624, 845– 858. https://doi.org/10.1016/j.scitotenv.2017.12.176

Ameli, A. A., Beven, K., Erlandsson, M., Creed, I. F., McDonnell, J. J., & Bishop, K. (2017). Primary weathering rates, water transit times, and concentration-discharge relations: A theoretical analysis for the critical zone. *Water Resources Research*, 53, 942– 960. https://doi.org/10.1002/2016wr019448

Andrews, D. M., Lin, H., Zhu, Q., Jin, L. X., & Brantley, S. L. (2011). Hot spots and hot moments of dissolved organic carbon export and soil organic carbon storage in the Shale Hills Catchment. *Vadose Zone Journal*, 10(3), 943– 954. https://doi.org/10.2136/vzj2010.0149

Bao, C., Li, L., Shi, Y., & Duffy, C. (2017). Understanding watershed hydrogeochemistry: 1. Development of RT-Flux-PIHM. *Water Resources Research*, 53, 2346– 2367. https://doi.org/10.1002/2016WR018935

Barlage, M., Chen, F., Tewari, M., Ikeda, K., Gochis, D., Dudhia, J., Rasmussen, R., Livneh, B., Ek, M., & Mitchell, K. (2010). Noah land surface

model modifications to improve snowpack prediction in the Colorado Rocky Mountains. *Journal of Geophysical Research-Atmospheres*, 115(D22), 115. https://doi.org/10.1029/2009jd013470

Basu, N. B., Destouni, G., Jawitz, J. W., Thompson, S. E., Loukinova, N. V., Darracq, A., Zanardo, S., Yaeger, M., Sivapalan, M., & Rinaldo, A. (2010). Nutrient loads exported from managed catchments reveal emergent biogeochemical stationarity. *Geophysical Research Letters*, 37, L23404. https://doi.org/10.1029/2010GL045168

Beck, H. E., van Dijk, A. I. J. M., Miralles, D. G., de Jeu, R. A. M., Bruijnzeel, L. A., McVicar, T. R., & Schellekens, J. (2013). Global patterns in base flow index and recession based on streamflow observations from 3394 catchments. *Water Resources Research*, 49, 7843– 7863. https://doi.org/10.1002/2013WR013918

Berghuijs, W. R., Woods, R. A., & Hrachowitz, M. (2014). A precipitation shift from snow towards rain leads to a decrease in streamflow. *Nature Climate Change*, 4(7), 583– 586. https://doi.org/10.1038/nclimate2246

Bhat, S. A., Meraj, G., & Pandit, A. K. (2016). Assessing the influence of stream flow and precipitation regimes on water quality of the major inflow stream of Wular Lake in Kashmir Himalaya. *Arabian Journal of Geosciences*, 9(1), 50. https://doi.org/10.1007/s12517-015-2083-1

Bishop, K., Seibert, J., Köhler, S., & Laudon, H. (2004). Resolving the double paradox of rapidly mobilized old water with highly variable responses in runoff chemistry. *Hydrological Processes*, 18(1), 185– 189. https://doi.org/10.1002/hyp.5209

Bowes, M. J., House, W. A., Hodgkinson, R. A., & Leach, D. V. (2005). Phosphorus–discharge hysteresis during storm events along a river catchment: The River Swale, UK. *Water Research*, 39(5), 751– 762. https://doi.org/10.1016/j.watres.2004.11.027

Bowes, M. J., Smith, J. T., & Neal, C. (2009). The value of high-resolution nutrient monitoring: A case study of the River Frome, Dorset, UK. *Journal of Hydrology*, 378(1-2), 82– 96. https://doi.org/10.1016/j.jhydrol.2009.09.015

Boyer, E. W., Hornberger, G. M., Bencala, K. E., & McKnight, D. (1996). Overview of a simple model describing variation of dissolved organic carbon in an upland catchment. *Ecological Modelling*, 86(2-3), 183– 188. https://doi.org/10.1016/0304-3800(95)00049-6

Boyer, E. W., Hornberger, G. M., Bencala, K. E., & Mcknight, D. M. (1997). Response characteristics of DOC flushing in an alpine catchment. *Hydrological Processes*, 11(12), 1635– 1647. https://doi.org/10.1002/(SICI)1099-1085(19971015)11:12<1635::AID-HYP494>3.0.CO;2-H

Brantley, S. L., Kubicki, J. D., & White, A. F. (2008). *Kinetics of water-rock interaction*. https://doi.org/10.1007/978-0-387-73563-4.

Carroll, R. W. H., Bearup, L. A., Brown, W., Dong, W., Bill, M., & Willlams, K. H. (2018). Factors controlling seasonal groundwater and solute flux from snow-dominated basins. *Hydrological Processes*, 32(14), 2187– 2202. https://doi.org/10.1002/hyp.13151

Chen, F., & Zhang, Y. (2009). On the coupling strength between the land surface and the atmosphere: From viewpoint of surface exchange coefficients. *Geophysical Research Letters*, 36, L10404. https://doi.org/10.1029/2009GL037980

Chiou, C. T., Lee, J. F., & Boyd, S. A. (1990). The surface-area of soil organic-matter. *Environmental Science & Technology*, 24(8), 1164– 1166. https://doi.org/10.1021/es00078a002

Claassen, H. C., & Halm, D. R. (1996). Estimates of evapotranspiration or effective moisture in Rocky Mountain watersheds from chloride ion concentrations in stream baseflow. *Water Resources Research*, 32(2), 363–372. https://doi.org/10.1029/95wr03111

Clow, D. W., & Mast, M. A. (2010). Mechanisms for chemostatic behavior in catchments: Implications for CO_2 consumption by mineral weathering. *Chemical Geology*, 269(1-2), 40– 51. https://doi.org/10.1016/j.chemgeo.2009.09.014

Creed, I. F., & Band, L. E. (1998). Export of nitrogen from catchments within a temperate forest: Evidence for a unifying mechanism regulated by variable source area dynamics. *Water Resources Research*, 34(11), 3105– 3120. https://doi.org/10.1029/98WR01924

Creed, I. F., Band, L. E., Foster, N. W., Morrison, I. K., Nicolson, J. A., Semkin, R. S., & Jeffries, D. S. (1996). Regulation of nitrate-N release from temperate forests: A test of the N flushing hypothesis. *Water Resources Research*, 32(11), 3337– 3354. https://doi.org/10.1029/96WR02399

Duffy, C., Shi, Y., Davis, K., Slingerland, R., Li, L., Sullivan, P. L., Goddéris, Y., & Brantley, S. L. (2014). Designing a suite of models to explore critical zone function. *Procedia Earth and Planetary Science*, 10, 7– 15. https://doi.org/10.1016/j.proeps.2014.08.003

Duncan, J. M., Band, L. E., & Groffman, P. M. (2017). Variable nitrate concentration–discharge relationships in a forested watershed. *Hydrological Processes*, 31(9), 1817– 1824. https://doi.org/10.1002/hyp.11136

Evans, C., & Davies, T. D. (1998). Causes of concentration/discharge hysteresis and its potential as a tool for analysis of episode hydrochemistry. *Water Resources Research*, 34(1), 129– 137. https://doi.org/10.1029/97WR01881

Fatichi, S., Vivoni, E. R., Ogden, F. L., Ivanov, V. Y., Mirus, B., Gochis, D., Downer, C. W., Camporese, M., Davison, J. H., & Ebel, B. (2016). An overview of current applications, challenges, and future trends in distributed process-

based models in hydrology. *Journal of Hydrology*, 537, 45– 60. https://doi.org/10.1016/j.jhydrol.2016.03.026

Godsey, S. E., Kirchner, J. W., & Clow, D. W. (2009). Concentration–discharge relationships reflect chemostatic characteristics of US catchments. *Hydrological Processes*, 23(13), 1844– 1864. https://doi.org/10.1002/hyp.7315

Grathwohl, P., Rügner, H., Wöhling, T., Osenbrück, K., Schwientek, M., Gayler, S., Wollschläger, U., Selle, B., Pause, M., & Delfs, J.-O. (2013). Catchments as reactors: A comprehensive approach for water fluxes and solute turnover. *Environmental Earth Sciences*, 69(2), 317– 333. https://doi.org/10.1007/s12665-013-2281-7

Gurdak, J. J. (2017). GROUNDWATER Climate-induced pumping. *Nature Geoscience*, 10(2), 71– 72. https://doi.org/10.1038/ngeo2885

Hagedorn, F., Bucher, J. B., & Schleppi, P. (2001). Contrasting dynamics of dissolved inorganic and organic nitrogen in soil and surface waters of forested catchments with Gleysols. *Geoderma*, 100(1-2), 173– 192. https://doi.org/10.1016/S0016-7061(00)00085-9

Hamamoto, S., Moldrup, P., Kawamoto, K., & Komatsu, T. (2010). Excluded-volume expansion of Archie's law for gas and solute diffusivities and electrical and thermal conductivities in variably saturated porous media. *Water Resources Research*, 46, W06514. https://doi.org/10.1029/2009WR008424

Hararuk, O., Smith, M. J., & Luo, Y. (2015). Microbial models with data-driven parameters predict stronger soil carbon responses to climate change. *Global Change Biology*, 21(6), 2439– 2453. https://doi.org/10.1111/gcb.12827

Haygarth, P., Turner, B. L., Fraser, A., Jarvis, S., Harrod, T., Nash, D., Halliwell, D., Page, T., & Beven, K. (2004). Temporal variability in phosphorus transfers: Classifying concentration–discharge event dynamics. *Hydrology and Earth System Sciences*, 8(1), 88– 97. https://doi.org/10.5194/hess-8-88-2004

Heidari, P., Li, L., Jin, L. X., Williams, J. Z., & Brantley, S. L. (2017). A reactive transport model for Marcellus shale weathering. *Geochimica et Cosmochimica Acta*, 217, 421– 440. https://doi.org/10.1016/j.gca.2017.08.011

Herndon, E., AlBashaireh, A., Singer, D., Chowdhury, T. R., Gu, B., & Graham, D. (2017). Influence of iron redox cycling on organo-mineral associations in Arctic tundra soil. *Geochimica et Cosmochimica Acta*, 207, 210– 231. https://doi.org/10.1016/j.gca.2017.02.034

Herndon, E., Dere, A. L., Sullivan, P., Norris, D., Reynolds, B., & Brantley, S. L. (2015a). Biotic controls on solute distribution and transport in headwater catchments. *Hydrology and Earth System Sciences*, 12(1), 213– 243. https://doi.org/10.5194/hessd-12-213-2015

Herndon, E. M., Dere, A. L., Sullivan, P. L., Norris, D., Reynolds, B., & Brantley, S. L. (2015b). Landscape heterogeneity drives contrasting concentration–discharge relationships in shale headwater catchments. *Hydrology and Earth System Sciences*, 19(8), 3333– 3347. https://doi.org/10.5194/hess-19-3333-2015

Herndon, E. M., Steinhoefel, G., Dere, A. L. D., & Sullivan, P. L. (2018). Perennial flow through convergent hillslopes explains chemodynamic solute behavior in a shale headwater catchment. *Chemical Geology*, 493, 413– 425. https://doi.org/10.1016/j.chemgeo.2018.06.019

Hoagland, B., Russo, T. A., Gu, X., Hill, L., Kaye, J., Forsythe, B., & Brantley, S. L. (2017). Hyporheic zone influences on concentration-discharge relationships in a headwater sandstone stream. *Water Resources Research*, 53, 4643– 4667. https://doi.org/10.1002/2016wr019717

Hornberger, G. M., Bencala, K. E., & McKnight, D. M. (1994). Hydrological controls on dissolved organic carbon during snowmelt in the Snake River near Montezuma, Colorado. *Biogeochemistry*, 25(3), 147– 165. https://doi.org/10.1007/bf00024390

Hubbard, S. S., Williams, K. H., Agarwal, D., Banfield, J., Beller, H., Bouskill, N., Brodie, E., Carroll, R., Dafflon, B., Dwivedi, D., Falco, N., Faybishenko, B., Maxwell, R., Nico, P., Steefel, C., Steltzer, H., Tokunaga, T., Tran, P. A., Wainwright, H., & Varadharajan, C. (2018). The East River, Colorado, Watershed: A mountainous community testbed for improving predictive understanding of multiscale hydrological–biogeochemical dynamics. *Vadose Zone Journal*, 17(1). https://doi.org/10.2136/vzj2018.03.0061

Hyer, K. E., Denver, J. M., Langland, M. J., Webber, J. S., Böhlke J., Hively, W. D., & Clune, J. W. (2016). Spatial and temporal variation of stream chemistry associated with contrasting geology and land-use patterns in the Chesapeake Bay watershed—Summary of results from Smith Creek, Virginia; Upper Chester River, Maryland; Conewago Creek, Pennsylvania; and Difficult Run, Virginia. 2010–2013Rep. 2328-0328, US Geological Survey.

Johnson, N. M., Likens, G. E., Bormann, F., Fisher, D., & Pierce, R. (1969). A working model for the variation in stream water chemistry at the Hubbard Brook Experimental Forest, New Hampshire. *Water Resources Research*, 5(6), 1353– 1363. https://doi.org/10.1029/WR005i006p01353

Kim, H., Bishop, J. K. B., Dietrich, W. E., & Fung, I. Y. (2014). Process dominance shift in solute chemistry as revealed by long-term high-frequency water chemistry observations of groundwater flowing through weathered argillite underlying a steep forested hillslope. *Geochimica et Cosmochimica Acta*, 140, 1– 19. https://doi.org/10.1016/j.gca.2014.05.011

King, K. W., Williams, M. R., Macrae, M. L., Fausey, N. R., Frankenberger, J., Smith, D. R., Kleinman, P. J. A., & Brown, L. C. (2015). Phosphorus transport

in agricultural subsurface drainage: A review. *Journal of Environmental Quality*, 44(2), 467– 485. https://doi.org/10.2134/jeq2014.04.0163

Li, L., Bao, C., Sullivan, P. L., Brantley, S., Shi, Y. N., & Duffy, C. (2017). Understanding watershed hydrogeochemistry: 2. Synchronized hydrological and geochemical processes drive stream chemostatic behavior. *Water Resources Research*, 53, 2346– 2367. https://doi.org/10.1002/2016wr018935

Li, L., Maher, K., Navarre-Sitchler, A., Druhan, J., Meile, C., Lawrence, C., Moore, J., Perdrial, J., Sullivan, P., Thompson, A., Jin, L., Bolton, E. W., Brantley, S. L., Dietrich, W. E., Mayer, K. U., Steefel, C. I., Valocchi, A., Zachara, J., Kocar, B., McIntosh, J., Tutolo, B. M., Kumar, M., Sonnenthal, E., Bao, C., & Beisman, J. (2017). Expanding the role of reactive transport models in critical zone processes. *Earth-Science Reviews*, 165, 280– 301. https://doi.org/10.1016/j.earscirev.2016.09.001

Li, L., Steefel, C. I., Williams, K. H., Wilkins, M. J., & Hubbard, S. S. (2009). Mineral transformation and biomass accumulation associated with uranium bioremediation at Rifle, Colorado. *Environmental Science & Technology*, 43(14), 5429– 5435. https://doi.org/10.1021/es900016v

Liu, Y., Wang, C., He, N., Wen, X., Gao, Y., Li, S., Niu, S., Butterbach-Bahl, K., Luo, Y., & Yu, G. (2017). A global synthesis of the rate and temperature sensitivity of soil nitrogen mineralization: Latitudinal patterns and mechanisms. *Global Change Biology*, 23(1), 455– 464. https://doi.org/10.1111/gcb.13372

Maher, K. (2011). The role of fluid residence time and topographic scales in determining chemical fluxes from landscapes. *Earth and Planetary Science Letters*, 312(1-2), 48– 58. https://doi.org/10.1016/j.epsl.2011.09.040

Manning, A. H., Verplanck, P. L., Mast, M., & Wanty, R. B. (2008). *Hydrogeochemical investigation of the standard mine vicinity*. Upper Elk Creek Basin, Colorado: U. S. Geological Survey.

McIntosh, J. C., Schaumberg, C., Perdrial, J., Harpold, A., Vázquez-Ortega, A., Rasmussen, C., Vinson, D., Zapata-Rios, X., Brooks, P. D., Meixner, T., Pelletier, J., Derry, L., & Chorover, J. (2017). Geochemical evolution of the Critical Zone across variable time scales informs concentration-discharge relationships: Jemez River Basin Critical Zone Observatory. *Water Resources Research*, 53, 4169– 4196. https://doi.org/10.1002/2016WR019712

Miller, M. P., Susong, D. D., Shope, C. L., Heilweil, V. M., & Stolp, B. J. (2014). Continuous estimation of baseflow in snowmelt-dominated streams and rivers in the Upper Colorado River Basin: A chemical hydrograph separation approach. *Water Resources Research*, 50, 6986– 6999. https://doi.org/10.1002/2013WR014939

Miller, M. P., Tesoriero, A. J., Capel, P. D., Pellerin, B. A., Hyer, K. E., & Burns, D. A. (2016). Quantifying watershed-scale groundwater loading and in-

stream fate of nitrate using high-frequency water quality data. *Water Resources Research*, 52, 330– 347. https://doi.org/10.1002/2015WR017753

Moatar, F., Abbott, B. W., Minaudo, C., Curie, F., & Pinay, G. (2017). Elemental properties, hydrology, and biology interact to shape concentration-discharge curves for carbon, nutrients, sediment, and major ions. *Water Resources Research*, 53, 1270– 1287. https://doi.org/10.1002/2016WR019635

Monod, J. (1949). The growth of bacterial cultures. *Annual Review of Microbiology*, 3(1), 371– 394. https://doi.org/10.1146/annurev.mi.03.100149.002103

Moon, S., Chamberlain, C., & Hilley, G. (2014). New estimates of silicate weathering rates and their uncertainties in global rivers. *Geochimica et Cosmochimica Acta*, 134, 257– 274. https://doi.org/10.1016/j.gca.2014.02.033

Musolff, A., Fleckenstein, J. H., Rao, P. S. C., & Jawitz, J. W. (2017). Emergent archetype patterns of coupled hydrologic and biogeochemical responses in catchments. *Geophysical Research Letters*, 44, 4143– 4151. https://doi.org/10.1002/2017gl072630

Musolff, A., Schmidt, C., Rode, M., Lischeid, G., Weise, S. M., & Fleckenstein, J. H. (2016). Groundwater head controls nitrate export from an agricultural lowland catchment. *Advances in Water Resources*, 96, 95– 107. https://doi.org/10.1016/j.advwatres.2016.07.003

Musolff, A., Schmidt, C., Selle, B., & Fleckenstein, J. H. (2015). Catchment controls on solute export. *Advances in Water Resources*, 86, 133– 146. https://doi.org/10.1016/j.advwatres.2015.09.026

Nagorski, S. A., Moore, J. N., McKinnon, T. E., & Smith, D. B. (2003). Geochemical response to variable streamflow conditions in contaminated and uncontaminated streams. *Water Resources Research*, 39(2), 1044. https://doi.org/10.1029/2001wr001247

Neagoe, A., Iordache, V., & Fărcăşanu, I. C. (2012). The role of organic matter in the mobility of metals in contaminated catchments. In *Bio-geo interactions in metal-contaminated soils*, edited, (pp. 297– 325). Berlin: Springer.

Pacific, V. J., Jencso, K. G., & McGlynn, B. L. (2010). Variable flushing mechanisms and landscape structure control stream DOC export during snowmelt in a set of nested catchments. *Biogeochemistry*, 99(1-3), 193– 211. https://doi.org/10.1007/s10533-009-9401-1

Peckhaus, A., Kiselev, A., Hiron, T., Ebert, M., & Leisner, T. (2016). A comparative study of K-rich and Na/Ca-rich feldspar ice-nucleating particles in a nanoliter droplet freezing assay. *Atmospheric Chemistry and Physics*, 16(18), 11,477– 11,496. https://doi.org/10.5194/acp-16-11477-2016

Rawls, W. J. (1983). Estimating soil bulk density from particle size analysis and organic matter content. *Soil Science*, 135(2), 123– 125. https://doi.org/10.1097/00010694-198302000-00007

Raymond, P. A., & Saiers, J. E. (2010). Event controlled DOC export from forested watersheds. *Biogeochemistry*, 100(1-3), 197– 209. https://doi.org/10.1007/s10533-010-9416-7

Roussiez, V., Probst, A., & Probst, J. L. (2013). Significance of floods in metal dynamics and export in a small agricultural catchment. *Journal of Hydrology*, 499, 71– 81. https://doi.org/10.1016/j.jhydrol.2013.06.013

Rumsey, C. A., Miller, M. P., Susong, D. D., Tillman, F. D., & Anning, D. W. (2015). Regional scale estimates of baseflow and factors influencing baseflow in the Upper Colorado River Basin. *Journal of Hydrology: Regional Studies*, 4, 91– 107. https://doi.org/10.1016/j.ejrh.2015.04.008

Runkel, R. L., Crawford, C. G., & Cohn, T. A. (2004). Load Estimator (LOADEST): A FORTRAN program for estimating constituent loads in streams and rivers. Rep. 2328-7055.

Rutherford, D. W., Chiou, C. T., & Kile, D. E. (1992). Influence of soil organic matter composition on the partition of organic compounds. *Environmental Science & Technology*, 26(2), 336– 340. https://doi.org/10.1021/es00026a014

Schwab, M. P., Klaus, J., Pfister, L., & Weiler, M. (2017). How runoff components affect the export of DOC and nitrate: A long-term and high-frequency analysis. *Hydrology and Earth System Sciences*, 1– 21. https://doi.org/10.5194/hess-2017-416

Seibert, J., Grabs, T., Köhler, S., Laudon, H., Winterdahl, M., & Bishop, K. (2009). Linking soil-and stream-water chemistry based on a Riparian Flow-Concentration Integration Model. *Hydrology and Earth System Sciences*, 13(12), 2287– 2297.

Shanklin, B., & Ryan, J. N. (2006). *Sources of metal contamination in the Coal Creek Watershed, Crested Butte, Gunnison County, Colorado: Part I*. University of Colorado at Boulder: Department of Civil, Environmental, and Architectural Engineering.

Shiller, A. M. (2010). Dissolved rare earth elements in a seasonally snow-covered, alpine/subalpine watershed, Loch Vale, Colorado. *Geochimica et Cosmochimica Acta*, 74(7), 2040– 2052.

Shmakin, B. M. (1979). Composition and structural state of K-feldspars from some US pegmatites. *American Mineralogist*, 64, 49– 56.

Stackpoole, S. M., Stets, E. G., Clow, D. W., Burns, D. A., Aiken, G. R., Aulenbach, B. T., Creed, I. F., Hirsch, R. M., Laudon, H., & Pellerin, B. A. (2017). Spatial and temporal patterns of dissolved organic matter quantity

and quality in the Mississippi River Basin, 1997–2013. *Hydrological Processes*, 31(4), 902– 915.

Streufert, R. K. (1999). *Geology and mineral resources of Gunnison County*. Colorado: Colorado Geological Survey, Department of Natural Resources.

Sullivan, P. L., Hynek, S. A., Gu, X., Singha, K., White, T., West, N., Kim, H., Clarke, B., Kirby, E., & Duffy, C. (2016). Oxidative dissolution under the channel leads geomorphological evolution at the Shale Hills catchment. *American Journal of Science*, 316(10), 981– 1026. https://doi.org/10.2475/10.2016.02

Sullivan, P. L., Stops, M. W., Macpherson, G. L., Li, L., Hirmas, D. R., & Dodds, W. K. (2018). How landscape heterogeneity governs stream water concentration-discharge behavior in carbonate terrains (Konza Prairie, USA). *Chemical Geology*. In press. https://doi.org/10.1016/j.chemgeo.2018.12.002

Taylor, R. G., Scanlon, B., Döll, P., Rodell, M., van Beek, R., Wada, Y., Longuevergne, L., Leblanc, M., Famiglietti, J. S., Edmunds, M., Konikow, L., Green, T. R., Chen, J., Taniguchi, M., Bierkens, M. F. P., MacDonald, A., Fan, Y., Maxwell, R. M., Yechieli, Y., Gurdak, J. J., Allen, D. M., Shamsudduha, M., Hiscock, K., Yeh, P. J. F., Holman, I., & Treidel, H. (2013). Ground water and climate change. *Nature Climate Change*, 3(4), 322– 329. https://doi.org/10.1038/Nclimate1744

Thomas, J. A., & Galey, J. T. (1982). Exploration and geology of the Mt. Emmons molybdenite deposits, Gunnison County, Colorado. *Economic Geology*, 77(5), 1085– 1104. https://doi.org/10.2113/gsecongeo.77.5.1085

Thompson, S., Basu, N., Lascurain, J., Aubeneau, A., & Rao, P. (2011). Relative dominance of hydrologic versus biogeochemical factors on solute export across impact gradients. *Water Resources Research*, 47, W00J05. https://doi.org/10.1029/2010WR009605

Trostle, K. D., Runyon, J. R., Pohlmann, M. A., Redfield, S. E., Pelletier, J., McIntosh, J., & Chorover, J. (2016). Colloids and organic matter complexation control trace metal concentration-discharge relationships in Marshall Gulch stream waters. *Water Resources Research*, 52, 7931– 7944. https://doi.org/10.1002/2016WR019072

Tunaley, C., Tetzlaff, D., Lessels, J., & Soulsby, C. (2016). Linking high-frequency DOC dynamics to the age of connected water sources. *Water Resources Research*, 52, 5232– 5247. https://doi.org/10.1002/2015WR018419

Vanni, M. J., Renwick, W. H., Headworth, J. L., Auch, J. D., & Schaus, M. H. (2001). Dissolved and particulate nutrient flux from three adjacent agricultural watersheds: A five-year study. *Biogeochemistry*, 54(1), 85– 114. https://doi.org/10.1023/a:1010681229460

Wang, G., Jagadamma, S., Mayes, M. A., Schadt, C. W., Steinweg, J. M., Gu, L., & Post, W. M. (2015). Microbial dormancy improves development and

experimental validation of ecosystem model. *ISME Journal*, 9(1), 226– 237. https://doi.org/10.1038/ismej.2014.120

Weiler, M., & McDonnell, J. R. J. (2006). Testing nutrient flushing hypotheses at the hillslope scale: A virtual experiment approach. *Journal of Hydrology*, 319(1-4), 339– 356. https://doi.org/10.1016/j.jhydrol.2005.06.040

Welch, L., & Allen, D. (2014). Hydraulic conductivity characteristics in mountains and implications for conceptualizing bedrock groundwater flow. *Hydrogeology Journal*, 22(5), 1003– 1026. https://doi.org/10.1007/s10040-014-1121-5

Wen, H., & Li, L. (2017). An upscaled rate law for magnesite dissolution in heterogeneous porous media. *Geochimica et Cosmochimica Acta*, 210, 289–305. https://doi.org/10.1016/j.gca.2017.04.019

Wen, H., & Li, L. (2018). An upscaled rate law for mineral dissolution in heterogeneous media: The role of time and length scales. *Geochimica et Cosmochimica Acta*, 235, 1– 20. https://doi.org/10.1016/j.gca.2018.04.024

Wen, H., Li, L., Crandall, D., & Hakala, A. (2016). Where lower calcite abundance creates more alteration: Enhanced rock matrix diffusivity induced by preferential dissolution, *Energy & Fuels*, 30(5), 4197– 4208.

White, A. F., & Blum, A. E. (1995). Effects of climate on chemical weathering in watersheds. *Geochimica et Cosmochimica Acta*, 59(9), 1729– 1747. https://doi.org/10.1016/0016-7037(95)00078-E

Wieder, W., Grandy, A., Kallenbach, C., & Bonan, G. (2014). Integrating microbial physiology and physio-chemical principles in soils with the MIcrobial-MIneral Carbon Stabilization (MIMICS) model. *Biogeosciences*, 11(14), 3899– 3917. https://doi.org/10.5194/bg-11-3899-2014

Wieder, W. R., Bonan, G. B., & Allison, S. D. (2013). Global soil carbon projections are improved by modelling microbial processes. *Nature Climate Change*, 3(10), 909– 912. https://doi.org/10.1038/nclimate1951

Winnick, M. J., Carroll, R. W. H., Williams, K. H., Maxwell, R. M., Dong, W., & Maher, K. (2017). Snowmelt controls on concentration-discharge relationships and the balance of oxidative and acid-base weathering fluxes in an alpine catchment, East River, Colorado. *Water Resources Research*, 53, 2507– 2523. https://doi.org/10.1002/2016WR019724

Winterdahl, M., Erlandsson, M., Futter, M. N., Weyhenmeyer, G. A., & Bishop, K. (2014). Intra-annual variability of organic carbon concentrations in running waters: Drivers along a climatic gradient. *Global Biogeochemical Cycles*, 28, 451– 464. https://doi.org/10.1002/2013GB004770

Wolery, T. J. (1992). *EQ 3/6, a software package for geochemical modeling of aqueous systems: Package overview and installation guide (version 7.0)*. Livermore, CA: Lawrence Livermore National Laboratory. https://doi.org/10.2172/138894

Woodruff, L., Cannon, W. F., Smith, D. B., & Solano, F. (2015). The distribution of selected elements and minerals in soil of the conterminous United States. *Journal of Geochemical Exploration*, 154, 49– 60. https://doi.org/10.1016/j.gexplo.2015.01.006

Yan, Z. F., Liu, C. X., Todd-Brown, K. E., Liu, Y. Y., Bond-Lamberty, B., & Bailey, V. L. (2016). Pore-scale investigation on the response of heterotrophic respiration to moisture conditions in heterogeneous soils. *Biogeochemistry*, 131(1-2), 121– 134. https://doi.org/10.1007/s10533-016-0270-0

Zarnetske, J. P., Bouda, M., Abbott, B. W., Saiers, J., & Raymond, P. A. (2018). Generality of hydrologic transport limitation of watershed organic carbon flux across ecoregions of the United States. *Geophysical Research Letters*, 45(21), 11,702– 11,711. https://doi.org/10.1029/2018GL080005

Zhang, Q. (2018). Synthesis of nutrient and sediment export patterns in the Chesapeake Bay watershed: Complex and non-stationary concentration-discharge relationships. *Science of the Total Environment*, 618, 1268– 1283. https://doi.org/10.1016/j.scitotenv.2017.09.221

Zhou, T., Shi, P., Hui, D., & Luo, Y. (2009). Global pattern of temperature sensitivity of soil heterotrophic respiration (Q10) and its implications for carbon-climate feedback. *Journal of Geophysical Research*, 114, G02016. https://doi.org/10.1029/2008JG000850